
# Zentrum für Technomathematik

**Fachbereich 3 – Mathematik und Informatik**


## On a Prediction Model for Concrete Carbonation based on Moving Interfaces - Interface concentrated Reactions


**Michael Böhm** **Jörg Kropp**

**Adrian Muntean**



Report 03–03

**Berichte aus der Technomathematik**

**Report 03–03** **April 2003**

# On a Prediction Model for Concrete Carbonation based on Moving Interfaces - Interface concentrated Reactions

Michael Böhm* Jörg Kropp† Adrian Muntean‡

**Abstract**: We formulate a coupled pde-ode-model for the simultaneous determination of concentrations and position of the carbonation front in concrete samples. The model is based on a two-phase moving boundary formulation in $D$ dimensions ($D = 1, 2, 3$) which involves an additional relation at the front and a modified carbonation-reaction rate restricted to a (thin) reaction layer near the front.

The geometry and numerical input data are modeled on accelerated-carbonation experiment settings for Portland cement in the range of $RH = 65\%$ and $[CO_2] = 3vol\%$, although the model should be applicable to more general situations. Simulations show a good qualitative agreement with experimental data - despite some drastic simplifications. It is shown that the model captures essential features of the carbonation process.

**Key words**: Carbonation of concrete, accelerated carbonation, prediction model, mathematical modeling, moving boundary formulation, partial differential equations, simulations.

**Acknowledgments**: This work has been partially supported by the Deutsche Forschungsgemeinschaft (DFG) by a grant through Sonderschwerpunktprogramm (SPP) 1122.

# 1 Introduction and problem statement

## 1.1 The carbonation process

Structural reinforced concrete is a composite material, in which the reinforcing steel is embedded in concrete - a two phase material in itself, composed of aggregates and the hydrated cement paste matrix.

One of the major risks for reinforced concrete structures is the corrosion of the steel reinforcement after depassivation of its surface occurs. In sound concretes steel is protected from corrosion by passivation in a high alkaline environment ($pH \approx 13$ of the pore water) due to the presence of $Ca(OH)_2$. If $pH$ drops below approximately 10 (up to $pH = 8.3$ in the fully carbonated zone), then passivation is lost. There are several scenarios leading to such drops in $pH$. One is the occurrence of atmospheric $CO_2$ near the steel bars leading to

*ZeTeM, FB3(Mathematik), University of Bremen, Germany, e-mail: mbohm@math.uni-bremen.de
†Institut für Baustofftechnologie, Hochschule Bremen, Germany, e-mail: kropp@fbb.hs-bremen.de
‡ZeTeM, FB3(Mathematik), University of Bremen, Germany, e-mail: muntean@math.uni-bremen.de

the reaction, simplified as the overall carbonation reaction between $Ca(OH)_2$ and $CO_2$:

$$Ca(OH)_2 + CO_2 \rightarrow CaCO_3 + H_2O. \tag{1}$$

Besides $Ca(OH)_2$ there are other, important components of the cement paste matrix which will undergo carbonation, such as the $CSH$-phases. Since $Ca(OH)_2$ represents the bulk of the carbonatable species in concrete, in a first approximation we restrict ourselves in this note to $Ca(OH)_2$, although a quantitatively more stringent setting requires to take the other reactions into account as well. For a more detailed description of the whole scenario cf. Ref. [32] and of the carbonation reaction involving more species or more complex scenarios than (1) involving intermediate reactions (like the formation of $CO_3^{2-}$, e.g.) cf. Refs. [45, 46, 47, 60, 61], e.g. Ref. [41] provides a more general framework for dealing with *many* reactants. For simulations or more conceptually oriented modeling, many authors reduce their setting to (1), because $Ca(OH)_2$ is the major reactant in most practical situations, and it is immediately linked to the corrosion risk.

Aside from carbonation another reason for depassivation of the reinforcing steel bars is the occurrence of chloride ions at the steel surface.

In the presence of chlorides depassivation of the steel surface even occurs in non-carbonated concrete, however, carbonation significantly reduces the chloride ion concentration necessary for the breakdown - the so-called threshold concentration.

The mechanism of how the chloride ingress is affected by carbonation is not uniform: For some types of concrete and environmental conditions carbonation seems to slow down chloridization, very often it plays an accelerating role. Vice versa, the influence of chlorides on the carbonation reactions seems to be far less important. For papers dealing with the coupled problem of carbonation and chloride attack, we refer to Refs. [59, 60, 38, 10, 20], e.g.

**Remark 1** In this note we concentrate on a (new way of) modeling intended to predict the progress of carbonation with time. Chlorides will not play any role in this model (cf. Refs. [60, 59, 56, 20] for information on the interplay of carbonation and chloride attack). Moreover, besides restricting ourselves to carbonation of $Ca(OH)_2$, we assume the whole process as isothermal. In this note temperature plays only the role of a parameter, although the whole carbonation process is not isotherm and in real-life concrete structures (and thus: inside of concrete samples or concrete members) atmospheric temperatures might vary. Our approach is basically molecular rather than ionic, as customary in an essential part of the literature. For (more general) approaches involving ionic transport we refer to Samson et al, Ref. [55], and, in a related context, Marchand, Ref. [39].

This note has been inspired by a paper of Wittmann and Brieger (cf. Ref. [28]). In their expository note the authors discuss several carbonation scenarios leading to Stefan-problem type formulations of carbonation. On the more modeling side this note has been influenced by the books by Gatignol and Prud'homme, Ref. [19] and Gurtin, Ref. [21], where, among others, concepts of surface-based productions as limits of appropriate volume-based productions are discussed.

## 1.2 Specification of the setting

For the sake of definiteness we concentrate on a cylindrical sample of concrete which is exposed to $CO_2$(g)[1] and humidity from the environment. Fig. 1 shows a cross section of such a piece. Denote by $\Omega(t)$ the part of the concrete piece for which we model the carbonation process. $\Omega(t)$ might be a whole sample or a part of it (cf. Fig. 2a-c: the hatched regions).

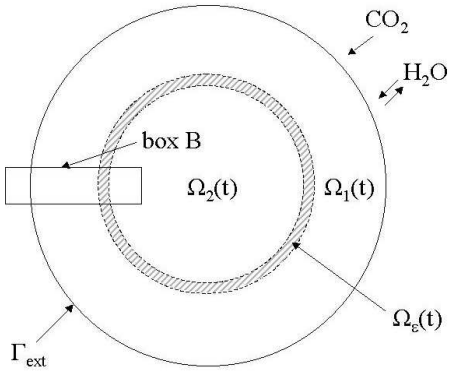


Figure 1: Cross section of a cylindrical concrete sample. The grey area indicates a zone $\Omega_\epsilon(t)$ of steep change in pH. $\Omega_2(t)$ is the uncarbonated zone. $\Omega_1(t)$ is the partially carbonated zone, $\Gamma_{ext}$ - the exterior boundary.

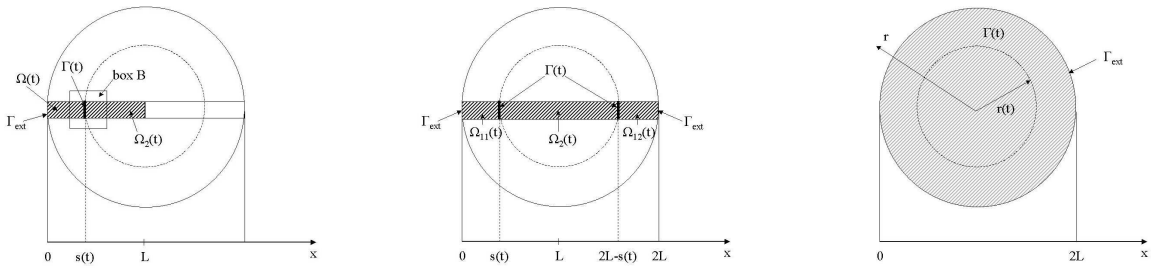


Figure 2: Cross sections of $\Omega(t)$. From left to right: Fig. 2a, Fig. 2b and Fig. 2c.

Introduction of time $t$ allows for possible changes of the shape and volume of the sample, although in *this* note the size and shape of (the macroscopic sample) $\Omega(t)$ is assumed to be constant.

The typical situation in a carbonation process can be summarized as follows: The concrete sample consists of a solid skeleton $\Omega_s(t)$ and the pore system $\Omega_p(t)$. $\Omega_p(t)$ is partially filled with water, which clings as a film, due to van der Walls forces, to the walls of the pores.

[1] $CO_2$(g) and $CO_2$(aq) denote the concentration of $CO_2$ in the gaseous phase and in the aqueous phase, respectively.

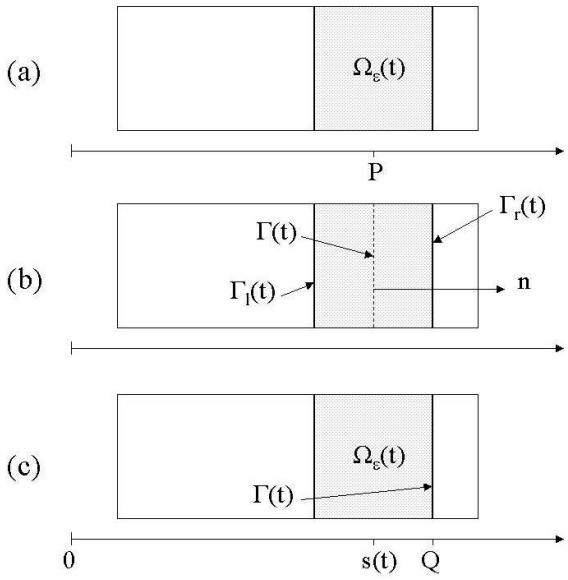


Figure 3: Disproportionally magnified box B from Fig. 2 with carbonation zone $\Omega_\epsilon(t)$ and two candidates for the definition of the 'carbonation front interface' $\Gamma(t)$ (center-lined surface or inner surface of $\Omega_\epsilon(t)$). The width of $\Omega_\epsilon(t)$ is $\epsilon$. From top to bottom: Fig. 5a, 5b, 5c.

The remaining parts of the pores are filled by water vapor and air. Vapor and water are summarized as *wetness or humidity*. Depending on the practical situation to be modeled, there might be transport of humidity through $\Omega(t)$ from or to the outside of $\Omega(t)$ or the wetness is assumed to be present (and its distribution to be known).

The air-filled pores serve as the main route through which $CO_2$ moves in $\Omega(t)$, since $CO_2$-diffusion in the water is considerably slower and thus negligible in this approach. Originally solid $Ca(OH)_2$ resides in $\Omega_s(t)$ (i.e. in the solid skeleton). Due to the water adsorbed at the pore walls, some parts of $Ca(OH)_2(s)$ dissolve into the water. Moreover, some part of the $CO_2$ moves from the air filled pore volume into the water, where it might react with dissolved $Ca(OH)_2$. Once $CaCO_3(aq)$ is formed, it precipitates very fast on the walls of the pores.

## 1.3 Carbonation zone, carbonated zones, carbonation fronts, carbonation speed and penetration depth

Examination of partially carbonated samples reveals a relatively narrow area over which $pH$ drops considerably. This is indicated by the grayish ring $\Omega_\epsilon(t)$ in Fig. 1. Usually this area is associated with the first occurrence (seen from the center of specimen) of the carbonation reaction(-s) taking place in or in the immediate neighborhood of this ring. Box B from Fig. 2a is magnified in Fig. 3.

Fig. 4 shows a typical $CO_2$-concentration profile. There are several possible explanations for the concentration drop (in $\Omega_\epsilon(t)$ or, in $1D$ : in $(R, Q)$) (cf. Fig. 4). We assume the next one: At any instant the bulk of the carbonation reaction takes place in $\Omega_\epsilon(t)$ leading to an almost complete consumption of the available $Ca(OH)_2(aq)$. Therefore $[CO_2]$ remains (almost) constant in the area between the point of entry in the concrete and $\Gamma_l$.

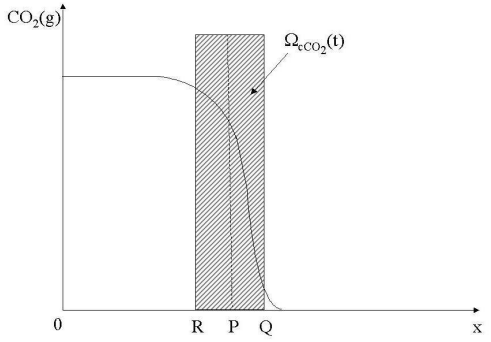


Figure 4: $CO_2$-concentration profile (cf. Ref. [27]) with reference to the coordinate system in Fig. 4. $P$ and $Q$ are possible candidates for the interface position.

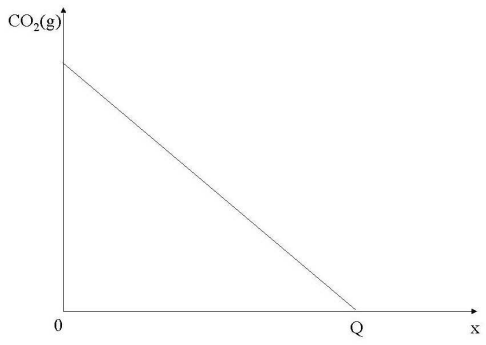


Figure 5: $CO_2$-concentration profile (cf. Ref. [26]) which does not give rise to the introduction of *interfacial* reaction *zones*. $Q$ defines the position of the reaction front.

What happens to $CO_2$ on its way from $\Gamma_{ext}$ to $\Omega_\epsilon(t)$? If there is $Ca(OH)_2(aq)$ in this area, produced by dissolution, e.g., then part of the $CO_2$ will be consumed by this reaction and the *rest* will move to $\Omega_\epsilon(t)$ to be available for the carbonation reaction. Otherwise *all* $CO_2$ will move into $\Omega_\epsilon(t)$. In this note we restrict ourselves to a conceptual and quantitative discussion of the latter case, for a discussion of the first one we refer to Ref. [8], e.g.

The middle line of the dotted area $\Omega_\epsilon(t)$ in Fig. 4 goes along with the middle line of $\Omega_\epsilon(t)$.

We will use Fig. 4 to introduce the notion of the *carbonation front* $\Gamma(t)$. There are conceptually (at least) two options for such an introduction - in Fig. 3a and 3b $\Gamma(t)$ is placed along the centerline of $\Omega_\epsilon(t)$, in Fig. 3c $\Gamma(t)$ closes $\Omega_\epsilon(t)$ at the right side. In this note we follow the suggestion from Fig. 3b.

For $CO_2$-profile as in Fig. 4, the concentration of $CO_2$ should vanish on the right surface of $\Omega_\epsilon(t)$ (Fig. 3a). The exact size of the width $\epsilon$ should be obtained from measurements (directly via $CO_2$). As it will turn out in section 4, the whole model is stable with respect to small changes of $\epsilon$ (cf. 3.11, remark a)).

Dual descriptions of $\Omega_\epsilon(t)$ in terms of high spatial $Ca(OH)_2$ concentration gradients or in the gradients of carbonation degree could be meaningful alternatives to the choice of $[CO_2]$.

Let $x$ be a point on $\Gamma(t)$, $n$ the normal to $\Gamma(t)$ at $x$ pointing into $\Omega_2(t)$ (cf. Fig. 3). The normal velocity $\dot{s}(x,t)$ of $\Gamma(t)$ (at $x$) is called the carbonation velocity (at $x$), the corresponding speed is the *carbonation speed (at x)*.

The model based on the limit case of the initial-carbonation reaction concentrated on $\Gamma(t)$ will be called *problem* $(P_\Gamma)$. The model based on describing carbonation where the initial-carbonation reaction is concentrated on $\Omega_\varepsilon(t)$ by $(P_{\Gamma\varepsilon})$. The full problem, $(P_{2\epsilon})$ of carbonation reactions on $\Omega_\varepsilon(t)$ as well as a posteriori carbonation reactions in the (partially) carbonated part will be dealt with later (cf. Ref. [8]).

With reference to Fig. 3b we call the region $\Omega_1(t)$ between the exterior boundary $\Gamma_{ext}$ and $\Gamma_l(t)$ the *carbonated region*, the rest, $\Omega_2(t)$, is the *uncarbonated region*. $\Omega_\epsilon(t)$ is the (main-) carbonation reaction zone, short: The carbonation zone.

**Remark 2** In the bulk of the engineering literature one uses $pH$ as the defining measure

for the carbonation zone. But: If there are/were further sources or sinks for $H^+$, then the definition in terms of $CO_2$ seems to be preferable. Moreover, once all concentrations are known, $pH$ can be computed. For carbonation a corresponding formula containing measurable data, is, under fairly general conditions, derived in Ref. [47].

**Remark 3** In this note we should clearly distinguish between the carbonation zone $\Omega_\epsilon(t)$, the (partially) carbonated zone $\Omega_1(t)$ and the (not yet) carbonated zone $\Omega_2(t)$. In general the bulk of reaction (1) takes place in $\Omega_\epsilon(t)$. In this note all of (1) is assumed to happen in $\Omega_\epsilon(t)$. Sometimes parts (or all) of $\Omega_1(t)$ are called 'fully carbonated zone'.

At any rate, in most situations is a small boundary layer of widths between a few mm and some cm. The width of $\Omega_\epsilon$ is even much smaller.

The carbonation-*penetration depth* $s$ is supposed to measure the distance between the position of the carbonation front and the external surface of the carbonated sample. In Fig. 2a,b. In Refs. [59, 60] $s(t)$ is defined by the isoline *carbonation degree* $= 0.9$. Other definitions place $s$ in the middle of the $pH$-drop zone or in the middle of the $CO_2$-drop zone (if there is such a zone! cf. Fig. 4a) or at the isoline $[CO_2] = \delta$, $\delta =$ very small or at $[CO_2] = 0$ (cf. Ref. [28], Model 2).

## 1.4 Accelerated-carbonation experiments (ace's)

In this note we will concentrate on a prediction model for the carbonation front in accelerated carbonation experiments (ace's). Ace's are used to predict the carbonation speed experimentally. The corresponding lab experiments (cf. Ref. [18, 58], e.g.) are based on real life situations where several of the parameters are considerably artificially changed in such a way that the experimentally observed carbonation speed is far higher than the corresponding one under natural conditions.

At the same time these experiments are used to check on the validity of some of the basic ideas and assumptions put into the models. Without acceleration the experiments would take years, with acceleration only a few weeks or months. We describe briefly the *ace* on which our numerical setting is based on.

In Fig. 6 hardened cylindrical concrete samples (height = 20 cm, diameter = 10 cm) are placed at time $t = 0$ in a carbonation chamber with constant relative humidity ($RH$) (here: $RH = 0.65$, in other experiments $RH \approx 0.4 - 0.8$) and constant $CO_2$-concentration (here: $3vol\%$, in other acceleration experiments: $1 - 2vol\%$, under real-life condition the $CO_2$-exposure is far lower, namely $0.03\ vol\%$). The samples remain in the chamber for a time $T$ (here: $T = 9$ weeks) after which they are removed from the chamber. The choice of $RH = 0.65$ is motivated by the experience that around this value of $RH$ carbonation advances at its highest speed. The whole cross section (cf. Fig. 2c) or parts of it (cf. hatched parts in Fig. 2a, b) constitute $\Omega(t)$. Before being put in the chamber, the cylinders have been pre-conditioned in such a way that the humidity in the sample corresponds almost to the humidity of the chamber.

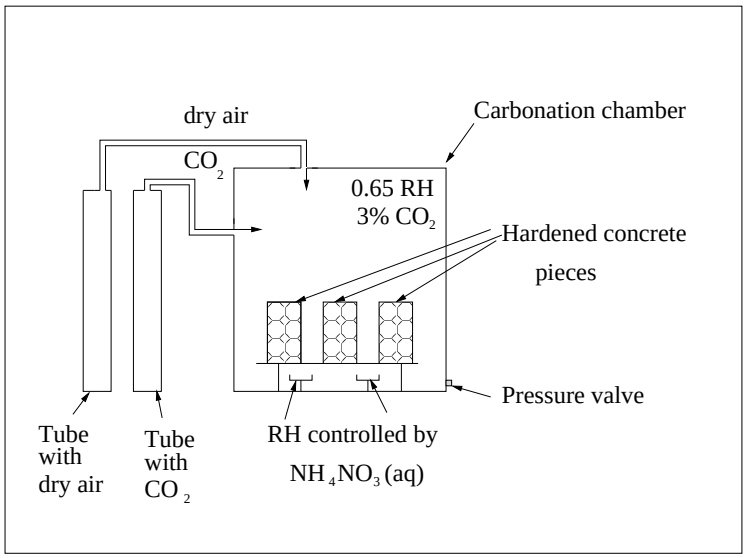


Figure 6: Schematic set-up of the accelerated carbonation experiment, cf. Ref. [58].

## 1.5 The aim and the character of the model

We formulate an (accelerated-) carbonation-experiment model allowing to calculate the relevant concentrations, the carbonation degree as well as the carbonation speed simultaneously. The model consists of coupled differential equations (ode and pde's) in $\Omega_1(t)$, $\Omega_\epsilon(t)$ and in $\Omega_2(t)$, respectively, supplemented by transmission conditions on $\Gamma(t)$ and an additional relation on $\Gamma(t)$ implicitly determining the carbonation speed. We will discuss two basic settings: Model $(P_{\Gamma\epsilon})$ and model $(P_\Gamma)$ (cf. section 2).

The **new modeling aspects** will be the *explicit introduction of a moving reaction front* and of an *additional equation for the determination of this front* and an *appropriate choice of the reaction rate*. In section 4 we present simulations based on the settings $(P_\Gamma)$ and $(P_{\Gamma\epsilon})$. They are then compared with accelerated carbonation experiments Ref. [58].

We want to show that this sort of modeling is capable of predicting essential features of $Ca(OH)_2$-based carbonation processes. Furthermore, we show that one has some freedom to formulate where *exactly* the carbonation reaction takes place - on a narrow strip or on a sharp interface.

## 1.6 The general formulation of the model

We deal with transport, reaction, dissolution, precipitation in the porous medium $\Omega(t)$ and in its parts $\Omega_k(t), k = 1, \epsilon, 2,\ \Gamma(t)$. Denote by $\phi$ the corresponding volumetric porosity (function) in $\Omega(t)$ ($\phi = \phi_k$ in $\Omega_k(t)$, respectively), $\widehat{\xi}_E = \widehat{\xi}_E(x,t)$ the mass concentration of a substance $E$ ($E = CO_2, CaCO_3$, $Ca(OH)_2$, moisture or others) being involved in the process under consideration, $\overline{\xi}_E := \phi\widehat{\xi}_E$ (i.e. $\int_{\Delta V}\overline{\xi}_E(x,t)dx$ = mass of $E$ in any control volume $\Delta V$), $j_E = j_E(x,t)$ - the flux (-density vector, modeling diffusive, thermally induced, con- or advective and charge-induced flows), $f_E = f_E(x,t)$ - the corresponding source or sink terms (modeling reaction, dissolution, precipitation, exchange between wet and dry

phases). The general equation describing all this is

$$\frac{\partial(\overline{\xi}_E(x,t))}{\partial t} + div_x j_E(x,t) = f_E(x,t),\ x \in \Omega \text{ ( or } x \in \Omega_i(t)),\ t > 0,\ i = 1,2. \qquad (2)$$

An essential part of the modeling consists in specifying $j_E$ and $f_E$ for the corresponding species, formulating transmission conditions on $\Gamma(t)$, initial and boundary conditions for $E$. Note that in the case of a carbonation reaction solely on $\Gamma(t)$, $f_{CaCO_3}$ might contain expressions describing distributions concentrated on $\Gamma(t)$, rather than functions on $\Omega(t)$, e.g.

# 2 Notations and definitions

## 2.1 Time and space. Models ($\mathbf{P}_\Gamma$) and ($\mathbf{P}_{\Gamma\varepsilon}$)

$\Omega(t)$ denotes the whole modeling area of the concrete sample (short: the (concrete) sample) at time $t$, $\Omega_1(t)$ is the carbonated part, $\Omega_2(t)$ - the uncarbonated part, $\Omega_\varepsilon(t)$ and $\Gamma(t)$, respectively, are the reaction-region and the reaction-interface (i.e. the surface in the middle of $\Omega_\varepsilon(t)$ between $\Omega_1(t)$ and $\Omega_2(t)$). Initial time $t = 0$ and final time $t = T$ are defined by the experiment (cf. section 1.4). $S := [0,T]$ is the basic time interval, $S' := (t, t + \Delta t]$ – an arbitrary subinterval of $S$. $t \in S$ and $x \in \Omega$ denote time and space variables, respectively.

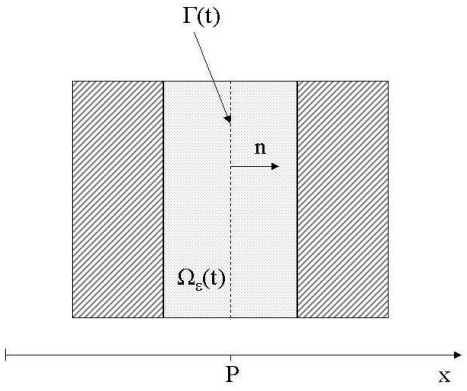


Figure 7: Geometry in model ($P_\Gamma$) and ($P_{\Gamma\epsilon}$).

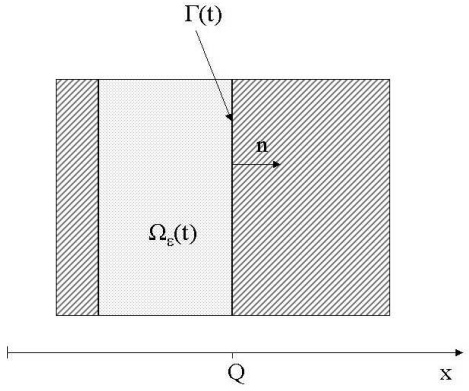


Figure 8: Another possible definition of the position of $\Gamma(t)$.

At initial time $t = 0$ we assume that there is already some (possibly very small) carbonated part $\Omega_{10}$ with non-zero volume. $\Omega'$ denotes a generic control volume in $\Omega(t)$, $n = n(x)$ is the unit normal on $\Gamma(t)$ pointing into $\Omega_2(t)$. Formally we have $(P_\Gamma)$=$(P_{\Gamma\epsilon=0})$.

The models $(P_\Gamma)$ and $(P_{\Gamma\varepsilon})$ are summarized in 1.4 and in 3.11, remark a), respectively.

## 2.2 Concentrations and flux densities

All concentrations are in $g/cm^3$ and they depend on position $x$ in the sample and on time $t \geq 0$. Some of the concentrations are relevant on all of $\Omega(t)$, some only on $\Omega_1(t)$ or on

$\Omega_2(t)$. In the latter case, the concentrations get an index 1 or 2, respectively. If they are relevant on either $\Omega_1(t)$ or on $\Omega_2(t)$, we do not use the extra index. If $\overline{c}_E = \overline{c}_E(x,t)$ and $\rho_E = \rho_E(x,t)$ denote the mass concentration and the mass density of a substance $E$ at $x$ and at time $t$, respectively, then $\widehat{c}_E := \frac{1}{\varrho_E}\overline{c}_E$ and $M_E$ stand for the corresponding volume fraction and the molar mass of $E$, respectively.

$\overline{w}$ := [moisture] (in all of $\Omega(t)$), $\overline{w}_0 := w(x,0)$ - initial moisture in $\Omega(0)$, $\overline{w}_k$, $\overline{w}_{0k}$ - corresponding restrictions of $w$ to $\Omega_k(t)$, $k = 1, 2$,

$\overline{c} := [CO_2(aq)]$ concentration of dissolved $CO_2$ in pore water[2] , $\overline{c}_0$ := initial concentration of $CO_2(aq)$ at $t = 0, \overline{c}_k$, $\overline{c}_{0k}$, - cf. line before[3],

$\overline{d} := [CO_2(g)]$ concentration of gaseous $CO_2$, $\overline{d}_0$ := initial concentration of $CO_2$(g) at $t = 0, \overline{d}_k$, $\overline{d}_{0k}$ - cf. footnotes 2, 3,

$\overline{h} := [Ca(OH)_2(aq)]$ concentration of aqueous calcium hydroxide, $\overline{h}_0$ := initially available $Ca(OH)_2(aq)$ in the wet part of $\Omega_2(0)$, $\overline{h}_k$, $\overline{h}_{0k}$ - cf. footnotes 2, 3,

$\overline{b}_w$ := concentration of dissolved $CaCO_3$ in $\Omega$, $\overline{b}_0 := \overline{b}(x,0), \overline{b_{wk}}$, $\overline{b}_{w0k}$ - cf. footnotes 2, 3,

$\overline{b}_s$ := concentration of precipitated $CaCO_3$ in $\Omega$, $\overline{b}_0 := \overline{b}(x,0), \overline{b_{sk}}$, $\overline{b}_{s0k}$ - cf. footnotes 2, 3,

$\overline{b} = [CaCO_3] := \phi_w b_w + \phi_s b_s :=$ total concentration of calcium carbonate in $\Omega_1(t)$.

In order to emphasize in which part ($\Omega_1(t)$ or $\Omega_2(t)$) a species (like water or $Ca(OH)_2(aq)$) is considered, we add an index to the concentrations, $\overline{w}_k(\cdot,t)$ stands for the water concentration in $\Omega_k(t)$ at time $t$, $k = 1, 2$, e.g.,

$\lambda_{\overline{c}}(t) := \lambda_{CO_2 out}(t) := CO_2(g)$-concentration at the boundary of the sample,

$\lambda_{\overline{w}}(t) := \lambda_{\overline{w}out}(t) :=$ humidity-mass concentration at the boundary of the sample, corresponding to the given exterior $RH$ (cf. ace in Ref. [58]).

$\lambda_{\overline{w}r}(t), \lambda_{\overline{h}r}(t)$ - corresponding (inner) boundary concentrations at the right side of the simulation area $\Omega(t)$ of the asymmetrical setting (cf. 3.8).

## 2.3 Further material and process functions and constants

The numerical values of the following constants will be introduced in sections 4 and 6.

$D_{\overline{w}k}$ - effective diffusion coefficient for moisture in $\Omega_k(t), k = 1, 2$,

$D_{\overline{c}k}$ - effective diffusion coefficient for $CO_2(aq)$ (cf. footnote 2),

$D_{\overline{d}k}$ - effective diffusion coefficient for $CO_2(g)$ (cf. footnote 2),

$D_{\overline{h}k}$ - effective diffusion coefficient for $Ca(OH)_2(aq)$ (cf. footnote 2),

$\phi_k$ - volumetric porosities in $\Omega_k(t), k = 1, 2$, with $\phi_{ks} = 1 - \phi_k$,

$\phi_w, \phi_a :=$ water- and air filled, respectively, fraction of the pores in $\Omega_1(t)$, $\phi_a + \phi_w = 1$,

$\eta_{R\Gamma}, \eta_{R\Gamma\varepsilon}$ - $\Gamma(t)$- and $\Omega_\varepsilon(t)$-concentrated surface- and volume-reaction rates for the reaction

[2] We introduce two *different* models: $(P_\Gamma)$ and $(P_{\Gamma\epsilon})$, both requiring consideration of concentrations on *different* domains. Thus, for the model $(P_\Gamma)$ the concentrations $\bar{c}, \bar{d}, \bar{b}$ are defined in $\Omega_1(t) \cup \Gamma(t)$ and $\bar{h}$ in $\Omega_2(t) \cup \Gamma(t)$. For the model $(P_{\Gamma\epsilon})$ the concentrations $\bar{c}, \bar{d}, \bar{b}$ are defined in $\Omega_1(t) \cup \Omega_\epsilon(t)$ and $\bar{h}$ in $\Omega_2(t) \cup \Omega_\epsilon(t)$. The diffusion coefficients are defined on that parts of $\Omega(t)$ where the corresponding species exist.

[3] All species $E = \bar{c}, \bar{d}, \bar{h}, \bar{b}$ have corresponding restrictions $E_k, E_{0k}$ in $\Omega_k(t)$, k=1,2.

(1) (cf. 3.1),

$P_H :=$ mass transfer coefficient in Henry's law, $Q_H :=$exchange factor in Henry's law (cf. section 3.3 below),

$P_{\overline{h}kdiss} :=$ factor in the dissolution law for $Ca(OH)_2$, $Q_{\overline{h}_{kdiss}}$, $\overline{h}_{keq} :=$ equilibrium concentration of $Ca(OH)_2$, $k = 1, 2$ (cf. 3.3 ),

$m^*_{Ca(OH)_2(s)}(x) :=$ initial (i.e. before dissolution starts) concentration at $x$ of $Ca(OH)_2(s)$ which is *available* for dissolution,

$S_{\overline{h}kdiss} :=$ switching factor (cf. 3.3),

$\kappa, \kappa_1$ - rate constants arising in Arrhenius' law.

# 3 The model

In this section we specify $\phi, j_E, f_E$ in section 1.6 and formulate the corresponding boundary, initial and, in particular, the interface conditions for $E := CO_2(aq), CO_2(g), Ca(OH)_2(aq)$ etc.

## 3.1 Reaction rates

The reaction (1) takes place in $\Omega(t)$ wherever there is sufficient $Ca(OH)_2(aq)$ and $CO_2(aq)$. We distinguish between the volume based reaction in $\Omega_1(t)$ away from $\Gamma(t)$ and the one near or even only at $\Gamma(t)$. In this note we assume the reaction at the carbonation front as complete, i.e. once (1) has taken place on $\Gamma(t)$ or in $\Omega_\varepsilon(t)$, we assume that there is no more carbonation going on in $\Omega_1(t)$. In Ref. [8] we will address the full problem by allowing subsequent dissolution of $Ca(OH)_2$ and reaction with $CO_2$ in the already (partially) carbonated zone.

In a situation with $\Gamma(t)$-based reactions it is not obvious what the 'correct' formal expression for the reaction rate, $\eta_{R\Gamma}$, is, since - to our knowledge - volume rates cannot be just used in very thin regions or even for surface based reactions without experimental evidence. Therefore we modify existing volume reaction rates by introducing two parameters $p$ and $q$.

There are (at least) two competing candidates for reactions rates. We mention the approach by Houst, Roelfstra, Wittmann, Saetta et al (cf. Refs. [26, 54] and also cf. Ref. [59], e.g.), which reads in our notation as

$$\text{rate for reaction (1)} = \eta_{vr} := \alpha A \exp(-\tfrac{E_0}{RT}) f_1 f_2 f_3,$$

where $\alpha$ is a constant, $T$ is the absolute temperature, $E_0$ is an activation energy, $A$ is a mean-collision number. $f_1$ is a scenario-switching factor describing the influence of relative humidity $c_w := RH$ on the reaction:

$$f_1(c_w) := \begin{cases} 0, & if \quad 0 \le c_w \le c_{w\,\min} \\ \frac{5}{2}(c_w - c_{w\,\min}), & if \quad c_{w\,\min} < c_w \le 0.9 \\ 1, & if \quad 0.9 < c_w \le 1 \end{cases},$$

where $c_{w\,\min} \approx 0.5$, $f_2 := 1 - \left(\frac{\overline{b}}{\overline{b}_{\max}}\right)^p$, $p = const. > 0$, $\overline{b}_{\max}$ := maximum amount of $CaCO_3$, $f_3 := \frac{\overline{c}}{\overline{c}_{\max}}$.

The other candidate for the reaction rate, $\eta_{sr}$, is the standard one for simple reactions, i.e.

$$\eta_{sr} := \kappa_{R\Gamma}\overline{c}\overline{h}.$$

In some way, $\eta_{vr}$ is a variation of the latter rate for a simple reaction $\eta_{sr}$ (cf. Steffens et al Ref. [59], p. 938).

In the present note we are mainly interested in showing that our approach works in principle (cf. 1.5) - therefore we prefer the seemingly simpler structure of $\eta_{sr}$ and use a generalization, $\eta_{R\Gamma}$, of $\eta_{sr}$ :

$$\eta_{R\Gamma} := \kappa_{R\Gamma}\overline{c}^p\overline{h}^q,\ p,q \in [0,2], \kappa_{R\Gamma} := \text{rate constant}. \tag{3}$$

In this case, $\overline{c}$ and $\overline{h}$ stand for surface concentrations. If one considers the reaction to take place on $\Omega_\varepsilon(t)$ rather than merely on $\Gamma(t)$, the reaction rate, $\eta_{R\Gamma\varepsilon}$, will be chosen as

$$\eta_{R\Gamma\varepsilon}(\cdot,t) := \chi_{\Omega_\varepsilon(t)}\kappa_{R\Gamma\varepsilon}\overline{c}^p(\cdot,t)\overline{h}^q(\cdot,t), \quad p,q \in [0,2],\ \kappa_{R\Gamma\varepsilon} := \text{rate constant}, \tag{4}$$

with $\chi_{\Omega_\varepsilon(t)}$ denoting the characteristic function of the set $\Omega_\varepsilon(t)$. We will employ the latter ansatz. $p$ and $q$ will be determined by a shooting argument.

**Remark 4** In order to clarify the meaning of $\eta_{R\Gamma}$, we recall the general concept of a surface reaction rate for reactions on a moving surface. To this end consider the amount of $CaCO_3$ produced on a moving surface, say on $\Gamma = \Gamma(\tau)$, over an arbitrary time interval $S' := (t, t+\Delta t]$ and let $\Omega' \subset \Omega$ be an arbitrary REV. Then $\mu_{R\Gamma}(S'\times\Omega') := \int_{S'}\int_{\Omega'\cap\Gamma(s)} c_{st\Gamma}\eta_{R\Gamma}d\sigma ds$ is the amount of $CaCO_3$ produced during $S'$ on that part of $\Gamma(s)$ which is at time $s$ in $\Omega'$. $c_{st\Gamma}$ denotes the appropriate stoichiometric coefficient of the reaction. In (1) it is $c_{st\Gamma} = 1$. If (1) is considered as a volume reaction then

$$\mu_{Rv}(S' \times \Omega') := \int_{S'}\int_{\Omega'} c_{stv}\eta_{Rv}dxds$$

is the amount of $CaCO_3$ produced in $\Omega'$ during $S'$ due to reaction, where $\eta_{Rv}$ is the corresponding *volume* based reaction rate. In (1) it is $c_{stv} = 1$.

Now consider the special situation in which the reaction is concentrated on a zone of width $\varepsilon$ around $\Gamma(t)$, $\Omega_\varepsilon := \left(-\frac{\varepsilon}{2}, \frac{\varepsilon}{2}\right) \times \Gamma(t)$, set $\mu^\varepsilon_{Rv} := \mu_{Rv}$ and $\eta_{Rv\varepsilon}(x) := \eta_{Rv}(x)$ if $x \in \Omega_\varepsilon$, and $\eta_{Rv\varepsilon}(x) := 0$ otherwise. (Note: In the case of carbonation, $\Omega_\varepsilon$ is the carbonation zone $\Omega_c$). Then the surface production measure $\mu_{R\Gamma}$ on $\Gamma(t)$ is defined by $\lim_{\varepsilon\to 0}\mu^\varepsilon_{Rv}(S'\times\Omega_\varepsilon) = \mu_{R\Gamma}(S'\times\Omega')$.

It is tacitly assumed in physical chemistry that the limit exists. This implies for the corresponding reaction rates

$$\varepsilon c_{stv}\eta^\varepsilon_{Rv} \to c_{st\Gamma}\eta_{R\Gamma} \text{ as } \varepsilon \to 0. \tag{5}$$

where convergence is to be understood in an appropriate sense. Hence, the production rate $\eta_{R\Gamma}$ on $\Gamma(t)$ is mathematically defined by the volume rates $\eta^\varepsilon_v$! Therefore, at a formal level, there is no freedom of choice of the structure of $\eta_{R\Gamma}$.

If one wishes to compare modeling concepts based on $\Gamma(t)$-concentrated with those based on $\Omega_\varepsilon(t)$-concentrated reactions, and, if both reactions are assumed to deliver the same amounts, (5) indicates that a proper scaling of the two reaction rates is given by

$$\varepsilon\eta^{\varepsilon}_{Rv} \approx \eta_{R\Gamma} \quad \text{or vice versa} \quad \eta^{\varepsilon}_{Rv} \approx \frac{1}{\varepsilon}\eta_{R\Gamma}. \tag{6}$$

## 3.2 Transport

In this note we will neglect all convective ('back pack', 'Huckepack') material transport, in the underlying ace the specimens had been in moisture at the start of the test. Also, in the case of carbonation, the corresponding transport is small. Moreover, we restrict ourselves to diffusive transport and assume it to be governed by the common linear variant of Fick's first law, i.e., with reference to (2)

$$j_E = -\widehat{D}_E\phi\nabla\xi_E, \tag{7}$$

where $D_E := \widehat{D}_E\phi$ is the corresponding effective diffusivity. For more comprehensive transport models we refer to Refs. [23, 30], e.g. In general, $D_E$ depends on porosity, $RH$, carbonation degree and others (cf. Refs. [34, 59, 52, 47], e.g.). In particular, this applies to $D_{CO_2}$ which is zero for very high $RH$ and becomes larger for higher fractions of pore air. For the sake of expositional simplicity we choose $D_E$ for all species $E$ as constant in each $\Omega_i(t), i = 1, 2$. That means that for $E := CO_2(g)$ we vary $D_{CO_2(g)}$ around values corresponding to the (high!) humidity outside the sample. The assumption of $D_{CO_2(g)} = const.$ in $\Omega_1(t)$ leads to a very week coupling of humidity and penetration depth which does not correspond to reality. Finally we note that there is only a very remote and academic chance, that (by the production of $H_2O$ via (1)) the humidity in $\Omega(t)$ is considerably higher than at the outside. Common understanding is that, in 1.4, this $H_2O$ is negligible with respect to counting towards additional humidity in $\Omega(t)$.

## 3.3 Dissolution, change of $CO_2$ from the air phase into the water phase, precipitation

The **exchange of $CO_2$** between the air and the wet phase is modeled by a Henry-law exchange term, i.e. by the sink term $f_{\overline{d}Henry} = -P_H(Q_H\overline{d} - \overline{c})$. This yields a source term for $CO_2$ in the wet phase, $f_{\overline{c}Henry} = -f_{\overline{d}Henry}$ (cf. Ref. [55] for some related arguments via homogenization). The **carbonation reaction** is modeled by using the reaction rate $\eta_{R\Gamma\epsilon}(\cdot, t)$ acting on $\Omega_\varepsilon(t)$ (cf. 3.1), which yields a sink term $f_{\overline{c}reac} := -\eta_{R\Gamma\epsilon}$ on $\Omega_\epsilon(t)$ for $CO_2$, and source terms $f_{\overline{b}_w reac} := +\eta_{R\Gamma\epsilon}$ for $CaCO_3$ as well as $f_{\overline{w}reac} := \eta_{R\Gamma\epsilon}$ for water - concentrated on the carbonation-reaction zone $\Omega_\varepsilon(t)$ in the wet phase of $\Omega_1(t)$. For the scenario with $\Gamma(t)$-concentrated reactions we have accordingly $f_{\overline{h}reac} = f_{\overline{c}reac} := -\eta_{R\Gamma}$, $f_{\overline{b}_w reac} := +\eta_{R\Gamma}$ on $\Gamma(t)$.

Taking (3), (4) and (6) into account, we choose $\eta_{R\Gamma} := \kappa_{R\Gamma}\overline{c}^p\overline{h}^q$, $\eta_{R\Gamma\epsilon} := \epsilon^{-1}\eta_{R\Gamma}$. The availability of $Ca(OH)_2(aq)$ in $\Omega_2(t)$ is governed by three factors: Initial availability of $Ca(OH)_2$ - determined by the initial concentration $\overline{h}_2(x, 0)$ in $\Omega_2(0)$, consumption at $\Gamma(t)$ and $\Omega_\varepsilon(t)$ and **dissolution of $Ca(OH)_2$** in $\Omega_k(t)$. The latter one is measured by the dissolution rate $f_{\overline{h}kdiss}$ which tries to minimize the deviation of the concentration $\overline{h}_k$ from

equilibrium-$Ca(OH)_2(aq)$-concentration $\overline{h}_{keq}$, i.e. $f_{\overline{h}kdiss} = P_{\overline{h}kdiss}(\overline{h}_k - \overline{h}_{keq}), k = 1, 2$ (linear non-instantaneous dissolution, equilibrium-deviation model).

A frequently used reasonable alternative and approximation for the dissolution rates is the assumption of constant (instantaneous) dissolution, i.e. $f_{\overline{h}kdiss} = Q_{\overline{h}kdiss} = const., k = 1, 2$. For other approaches modeling dissolution in our context we refer to Refs. [45, 36, 37, 48], e.g. Note that all dissolution rates underly a natural side condition: Once all $Ca(OH)_2(s)$ that *can* be dissolved is exhausted, $f_{\overline{h}kdiss}$ becomes zero. This can be formulated by introducing a switching factor

$$S_{\overline{h}kdiss}(x) = S_{\overline{h}kdiss}([Ca(OH)_2(s)\text{-available-for-dissolution at point } x] :=$$

$$= \begin{cases} 0 \text{ if } [Ca(OH)_2(s)\text{-available-for-dissolution at point } x] = 0 \\ 1 \text{ otherwise} \end{cases},$$

and $f_{\overline{h}kdiss} = S_{\overline{h}kdiss} P_{\overline{h}kdiss}(\overline{h}_k - \overline{h}_{keq})$ (non-instantaneous dissolution) and $f_{\overline{h}kdiss} = S_{\overline{h}kdiss} Q_{\overline{h}kdiss}$ (instantaneous-dissolution model), respectively.

The switching criterion can be reformulated in the following way: Let $m^*_{Ca(OH)_2(s)} = m^*_{Ca(OH)_2(s)}(x)$ denote the initial (i.e. before dissolution starts) concentration at $x$ of $Ca(OH)_2(s)$-available-for-dissolution.

$\int_0^t f_{\overline{h}kdiss}(x, \tau) d\tau$ is the concentration of all $Ca(OH)_2(aq)$ generated at the point $x$ during time $(0, t]$ by dissolution. Then: $[Ca(OH)_2(s)$-available-for- dissolution at point $x] = 0$, if $\int_0^t f_{\overline{h}kdiss}(x, \tau) d\tau \geq m^*_{Ca(OH)_2(s)}(x)$.

**Precipitation** will be modeled as instantaneous in the following sense: Once $CaCO_3(aq)$ is formed, it precipitates right away, i.e. $f_{\overline{b}_w prec} = -f_{\overline{b}_w reac}$, and therefore $f_{\overline{b}_s prec} = f_{\overline{b}_w reac}$.

## 3.4 Balance equations

### 3.4.1 Transport of $CO_2$ in the air phase of $\Omega_1(t) \cup \Omega_\epsilon(t)$

$$\frac{\partial \overline{d}}{\partial t} + div(j_{\overline{d}}) = f_{\overline{d}Henry} \quad \text{in } \Omega_1(t) \cup \Omega_\epsilon(t). \tag{8}$$

### 3.4.2 Transport and reaction of $CO_2$ in the wet phase of $\Omega_1(t) \cup \Omega_\epsilon(t)$

$$\frac{\partial \overline{c}}{\partial t} + \underbrace{div(j_{\overline{c}})}_{\text{cf. 3.5 !}} = f_{\overline{c}Henry} + f_{\overline{c}reac} \text{ in } \Omega_1(t) \cup \Omega_\epsilon(t). \tag{9}$$

### 3.4.3 Transport, reaction and dissolution of $Ca(OH)_2$ in the wet phase of $\Omega_2(t) \cup \Omega_\epsilon(t)$

$$\frac{\partial \overline{h}_k}{\partial t} + div(j_{\overline{h}k}) = f_{\overline{h}kdiss} + f_{\overline{h}kreac} \text{ in } \Omega_2(t) \cup \Omega_\epsilon(t). \tag{10}$$

### 3.4.4 Transport and reaction and precipitation of $CaCO_3$ in the wet phase of $\Omega_1(t) \cup \Omega_\epsilon(t)$

$$\frac{\partial \phi_{1w} \overline{b}_w}{\partial t} + \underbrace{div(j_{\overline{b}_w})}_{=0 \text{ (cf. 3.5)}} = f_{\overline{b}_w prec} + f_{\overline{b}_w reac} \text{ in } \Omega_1(t) \cup \Omega_\epsilon(t). \tag{11}$$

According to 3.3 we obtain for the precipitated $CaCO_3$

$$\frac{\partial \phi_{1s} \overline{b}_s}{\partial t} + \underbrace{div(j_{\overline{b}_s})}_{=0} = f_{\overline{b}_s prec} \quad \text{in } \Omega_1(t) \cup \Omega_\epsilon(t). \tag{12}$$

The total $CaCO_3$-content follows from

$$\frac{\partial \overline{b}}{\partial t} = f_{\overline{b}_w reac} \quad \text{in } \Omega_1(t) \cup \Omega_\epsilon(t). \tag{13}$$

Notice that, when discussing the model $(P_\Gamma)$, $\Omega_\epsilon$ should be dropped from the equations (9)-(12).

### 3.4.5 Transport and generation of $H_2O$ in $\Omega_k(t),\ k = 1, 2$

Since water is supposed to be in the whole sample, there is only one equation for the corresponding concentrations:

$$\frac{\partial \overline{w}}{\partial t} + div(j_{\overline{w}}) = f_{\bar{w} reac} \text{ in } \Omega(t). \tag{14}$$

According to the sharp-interface scenario, $f_{\overline{w} reac}$ is a distribution concentrated on $\Gamma(t)$! Note that the material parameters might be different in $\Omega_1(t)$ and $\Omega_2(t)$, in particular: $\phi = \phi(x,t)$ is $\phi_k$ if $x \in \Omega_k(t)$ and it enters (14) twice - via the flux term and via the definition of $\overline{w}$ (cf. section 1.6).

## 3.5 Remarks

(i) There are two different ways to model diffusive transport of $CO_2$ in the water phase.

(ia) Diffusion in water is very slow compared to diffusion in the air phase. Therefore some authors neglect the diffusion term $div(j_{\overline{c}})$ in 3.4.2. This reduces the pde in 3.4.2 to an ode (in $t$), in which $x$ becomes a parameter and for which no boundary conditions with respect to $x$ are needed. In this case the boundary conditions for $\overline{c}$ in 3.7 *cannot* be posed. The space variable $x$ is a parameter and only for $x \in \Gamma(t)$ and $x \in \Omega_\varepsilon(t)$, respectively, the reaction term becomes relevant.

(ib) Keeping diffusion of $CO_2$ in the wet phase in the model implies the necessity of boundary conditions for $CO_2$ in the wet phase.

(ii) Compared to precipitation and reaction, the diffusive transport of $Ca(OH)_2(aq)$ is also slow, hence one could possibly neglect the term $div(j_{\overline{h}})$ in $\Omega_2(t)$ (cf. [12, 54, 59], e.g.)

(iii) We call carbonation *complete* if all $CO_2$ in $\Omega_1(t)$ is consumed right away in $\Omega_\varepsilon(t)$ or at $\Gamma(t)$, respectively, and if *all* available $Ca(OH)_2$ is consumed by (1) in $\Omega_\varepsilon(t)$ and on $\Gamma(t)$, respectively. In particular this means that there is no $Ca(OH)_2$ available in $\Omega_1(t) \setminus \Omega_\varepsilon(t)$ or $\Omega_1(t) \setminus \Gamma(t)$, respectively. Therefore, for the case of $\Gamma(t)$-concentrated reactions we can drop the equation for $\overline{h}_1$ in 3.4.3. The quantitative consequences of this assumption for the speed of the carbonation front will be discussed in Ref. [8].

## 3.6 Boundary conditions at the outside of the sample

The setting in 1.4 gives rise to Dirichlet boundary data for $H_2O$, $CO_2(g)$ and $CO_2(aq)$ at the surface of $\Omega(t)$. $\overline{w}(0,t)$ is determined by the outside humidity. Furthermore, we assume $CO_2(g)$ and $CO_2(aq)$ in Henry-law equilibrium, i.e. with respect to section 3.2, the given outside $CO_2$-concentration $\lambda_{CO_2out}$ splits into two parts satisfying

$$\overline{c}(0,t) = Q_H \overline{d}(0,t), \overline{d}(0,t) + \overline{c}(0,t) = \lambda_{CO_2out}(t). \tag{15}$$

Therefore

$$\overline{c}(0,t) = \lambda_{\overline{d}}(t) := \frac{Q_H}{1+Q_H}\lambda_{CO_2out}(t), \quad \overline{d}(0,t) = \frac{1}{1+Q_H}\lambda_{CO_2out}(t). \tag{16}$$

See also Refs. [2, 6], e.g.

The boundary conditions for $\overline{w}$ are given by

$$\overline{w}(0,t) = \lambda_{\overline{w}out}(t). \tag{17}$$

Because of 3.5(iii) there is no need for boundary conditions at the outside of $\Omega(t)$ for $Ca(OH)_2(aq)$.

## 3.7 Boundary conditions associated with the carbonation zone $\Omega_\varepsilon(t)$ and at the carbonation front $\Gamma(t)$

We discuss the two settings, $(P_\Gamma)$ and $(P_{\Gamma\varepsilon})$, separately.

### 3.7.1 $(P_\Gamma)$ : Boundary conditions on $\Gamma(t)$

Since there is supposedly no $CO_2$ in $\Omega_2(t)$, there can't be any flow of $CO_2$ from $\Omega_1(t)$ into $\Omega_2(t)$, i.e.

$$j_{\overline{d}}(\cdot,t) \cdot n = 0 \text{ at } \Gamma(t), \tag{18}$$

where $n$ denotes the normal field at $\Gamma(t)$ pointing into $\Omega_2(t)$.

Dissolved calcium hydroxide enters $\Gamma(t)$ from $\Omega_2(t)$ and is there consumed by carbonation, i.e., with an argument as for the derivation of the classical Stefan-melting-problem (cf. Ref. [51], e.g.), the Rankine-Hugoniot conditions for moving interfaces (cf. Refs. [21, 62]) read as

$$j_{\overline{h}}(\cdot,t)\cdot(-n)=\eta_{R\Gamma}-\dot{s}(\cdot,t)\overline{h}(\cdot,t). \tag{19}$$

$CO_2(aq)$ from $\Omega_1(t)$ enters $\Gamma(t)$ and is consumed by carbonation, i.e.

$$j_{\overline{c}}(\cdot,t)\cdot n=\eta_{R\Gamma}+\dot{s}(\cdot,t)\overline{c}(\cdot,t). \tag{20}$$

For $CO_2(g)$ we assume

$$j_{\overline{d}}(\cdot,t)\cdot n=\dot{s}(\cdot,t)\bar{d}(\cdot,t). \tag{21}$$

Note: Clearly, this boundary condition is an idealization, as long as there is some $CO_2(g)$ at $\Gamma(t)$. In some way, equally suited are Dirichlet-boundary conditions for $CO_2(g)$, i.e. $\overline{d}(x,t)=0$ for $x\in\Gamma(t)$.

Finally, we assume a no-jump condition for $w$, i.e. $w(\cdot,t)$ is continuous across $\Gamma(t)$.

### 3.7.2 $(P_{\Gamma_\varepsilon})$ : Boundary conditions associated with the carbonation zone $\Omega_\varepsilon(t)$

The situation is depicted in Fig. 8. $Ca(OH)_2(aq)$ enters $\Omega_\varepsilon(t)$ by diffusion from $\Omega_2(t)$ and reacts in $\Omega_\varepsilon(t)$. Since in this setting we disregard any other carbonation (such as in the rest of $\Omega_1(t)$), we have to require

$$j_{\overline{h}}(\cdot,t)\cdot(-n')=0 \text{ at } \Gamma_l(t). \tag{22}$$

Here $n'$ denotes the normal field on $\Gamma_l(t)$ pointing towards $\Omega_2(t)$.

Similarly $CO_2(aq)$ (as well as $CO_2(g)$) enters $\Omega_\varepsilon(t)$ from the rest of $\Omega_1(t)$ and reacts. Since there is no reaction in $\Omega_2(t)$, we have to require

$$j_{\overline{c}}(\cdot,t)\cdot n=j_{\overline{d}}(\cdot,t)\cdot n=0 \text{ at } \Gamma_r(t). \tag{23}$$

## 3.8 Further boundary condition

We distinguish between three settings corresponding to Fig. 2a-c .

### 3.8.1 Boundary conditions with reference to Fig. 2a

Taking into account the symmetry with respect to $x=L$, one has

$$\left.\begin{aligned}-j_{\overline{h}}(x,t)\cdot n(x)&=0\\ -j_{\overline{w}}(x,t)\cdot n(x)&=0\end{aligned}\right\}\ \text{at } x=L. \tag{24}$$

An alternative used by some authors is

$$\left.\begin{array}{l}\overline{h}(x,t) = \lambda_{\overline{h}r}(t) \\ \overline{w}(x,t) = \lambda_{\overline{w}r}(t)\end{array}\right\} \text{ at } x = L. \tag{25}$$

Here $\lambda_{\overline{h}r}(t)$ is a dissolution source centered at $x = L$.

### 3.8.2 Boundary conditions with reference to Fig. 2b

No further boundary conditions are needed.

### 3.8.3 Boundary conditions with reference to Fig. 2c

The only (obvious) requirement is that all concentrations and their space derivatives are finite at $r = 0$.

## 3.9 An equation for the speed of the interface

### 3.9.1 Case 1: Model $(P_\Gamma)$ – $\Gamma(t)$-concentrated carbonation reaction. $\Gamma(t)$ with small curvature

Consider the advancement of $\Gamma(t)$ over a time interval $S' := (t, t + \Delta t]$ (cf. Fig. 9).

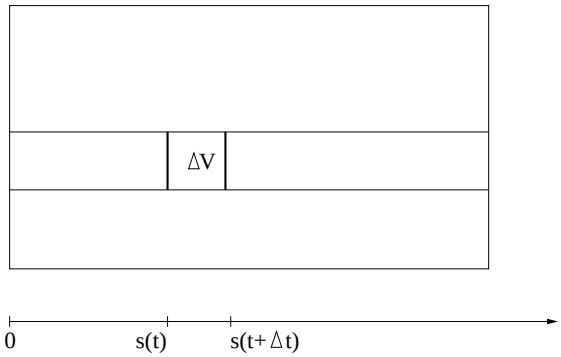


Figure 9: $\Delta V$ in 1D setting.

The amount of $Ca(OH)_2$ consumed during $S'$ in $\Delta V$ is $\Delta s \overline{h}(x,t')\,|\Gamma(t')|$ for some $t' \in (t, t + \Delta t]$ (before carbonation). After $t + \Delta t'$ this amount is removed by (1). The removed amount follows from the reaction rate as

$$\int_{S'} \int_{\Gamma(\tau)} \eta_{R\Gamma}(x,\tau) d\sigma d\tau = |\Gamma(t'')|\,\Delta t \eta_{R\Gamma}(x,t'') \tag{26}$$

for some $t'' \in (t, t + \Delta t]$. Therefore $\frac{\Delta s}{\Delta t} = \frac{|\Gamma(t'')|}{|\Gamma(t')|} \frac{1}{\overline{h}(x,t')} \eta_{R\Gamma}(x,t'')$. Letting $\Delta t \to 0$ on both sides, one arrives at

$$\dot{s}(x,t) = \frac{1}{\overline{h}(x,t)} \eta_{R\Gamma}(x,t), x \in \Gamma(t), t > 0. \tag{27}$$

The usual modifications of the argument for $D > 1$ yield (27), too (cf. Ref. [51], e.g.).

Note: (27) yields for $D := 1$ the

$$\text{penetration depth}: \quad s(t) = s_0 + \int_0^t \frac{1}{\overline{h}(x,\tau)} \eta_{R\Gamma}(x,\tau) d\tau. \tag{28}$$

Unfortunately, this is not an explicit formula for $s(t)$, since the concentrations and $s(t)$ are coupled via (3) and (4) and the equations in 3.4 which are formulated on $\Omega_1(t)$ which depends on $s(t)$!

### 3.9.2 Case 2: $\Omega(t)$ is a cylinder, $\Gamma(t)$ is a cylinder mantle. Completely symmetric setting as in Fig. 2c

We consider the advancement of $\Gamma(t)$ as in Fig. 9.

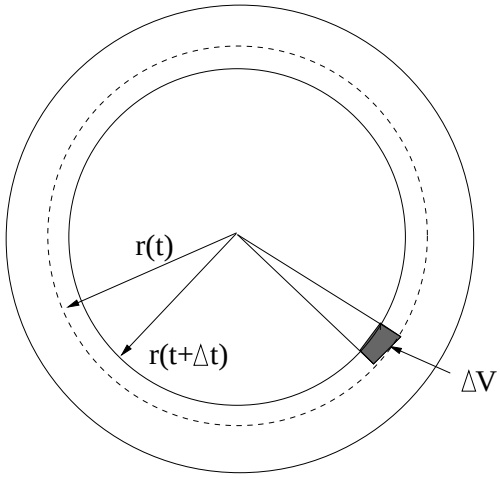


Figure 10: Advancement of $\Gamma(t)$ in 2D setting with radial symmetry.

The whole argument is identical with the one for the previous case. Repeating the same argument leading to (26) in polar coordinates and observing the angular symmetry of the setting one obtains (25).

### 3.9.3 Case 3: Model ($P_{\Gamma\epsilon}$) – $\Omega_\varepsilon(t)$-concentrated carbonation reaction

In analogy to 3.9.1 and using (6) we *postulate*

$$\dot{s}(t) = \left[\frac{1}{\varepsilon}\int_{\Omega_\varepsilon(t)} \overline{h}(x,t)dx\right]^{-1} \int_{\Omega_\varepsilon(t)} \eta_{R\Gamma\varepsilon}(x,t)dx. \tag{29}$$

## 3.10 Initial conditions

Initial conditions for $Ca(OH)_2$ are based on the ace-setting (Ref. [58]), a (here not used) theoretical background for the initial values of $Ca(OH)_2$ (as well as of the major $CSH$-phases) could be provided by Ref. [46], e.g.). The initially carbonated part $\Omega_{01}$ as well as the other initial conditions are supposed to be known (for calculations see section 4), i.e.

$$\left.\begin{array}{l} \overline{w_k}(x,0) = \overline{w}_{0k}(x), k = 1,2 \\ \overline{b_j}(x,0) = \overline{b}_{0j}(x), j = a, w \\ \overline{c}(x,0) = \overline{c}_0(x) \\ \overline{d}(x,0) = \overline{d}_0(x) \\ \overline{h}(x,0) = \overline{h}_0(x) \end{array}\right\} \tag{30}$$

$$\Omega_1(0) = \Omega_{10}, \Omega_2(0) = \Omega_{20} := \Omega \setminus \Omega_{10}. \tag{31}$$

## 3.11 Remarks

**a)** The model $(P_\Gamma)$ (i.e. equations in 3.4 together with 3.5, initial conditions in 3.10, boundary conditions in 3.6, 3.7.1 and 3.1-3.3, and also, the equation (27) for the interface speed) is well posed (cf. Refs. [9, 7], i.e. for given data (initial and boundary values, constants in the dissolution and precipitation laws, reactions constants, reaction exponents $p$ and $q$, $\Omega_{01}$ etc. there is exactly one solution vector $X := (s, \overline{w}, \overline{b}, \overline{c}, \overline{d}, \overline{h})$. The same applies for the model $(P_{\Gamma\varepsilon})$ (i.e. 3.1-3.3, 3.4 and 3.5, 3.6, 3.7.2 (!), 3.10 and 3.9). Denote by $X_\varepsilon := (s_\varepsilon, \overline{w}_\varepsilon, \overline{b}_\varepsilon, \overline{c}_\varepsilon, \overline{d}_\varepsilon, \overline{h}_\varepsilon)$ the corresponding solution vector with respect to the same data. Recall that by 3.1 and (28) the reaction rate depends on some concentrations, $\eta_{R\Gamma\varepsilon}(x,t) = \widetilde{\eta}_{R\Gamma\varepsilon}(\overline{c}_\varepsilon(x,t), \overline{h}_\varepsilon(x,t))$, where

$$\widetilde{\eta}_{R\Gamma\varepsilon}(r,s) := \kappa_{R\Gamma\varepsilon} r^p s^q \tag{32}$$

and

$$\eta_{R\Gamma}(x,t) = \widetilde{\eta}_{R\Gamma}(\overline{c}(x,t), \overline{h}(x,t)) \tag{33}$$

with $\widetilde{\eta}_{R\Gamma}(r,s) := \kappa_{R\Gamma}\ r^p s^q$ and assume $\varepsilon\widetilde{\eta}_{R\Gamma\varepsilon} \overset{\varepsilon\to 0}{\to} \widetilde{\eta}_{R\Gamma}$, then (i) $X_\varepsilon \overset{\varepsilon\to\varepsilon_0}{\to} X_{\varepsilon_0}$ and even (ii) $X_\varepsilon \overset{\varepsilon\to 0}{\to} X$ (theoretically and numerically). (i) implies that small changes of the data- and model input do not change the solution output. In particular, a change of the exact width $\varepsilon$ of $\Omega_\varepsilon(t)$ will not change the general outcome $X_\varepsilon$ very much. (ii) suggests that $(P_{\Gamma\varepsilon})$ can be considered as an approximation of $(P_\Gamma)$ or, vice versa, $(P_\Gamma)$ can be considered as an approximation for $(P_{\Gamma\varepsilon})$ for small $\varepsilon$.

**b)** From a numerical point of view, $(P_{\Gamma\epsilon})$ is generally easier to handle than $(P_\Gamma)$, since the evaluation of the $\Gamma(t)$-concentrated reaction terms relies on only a single point (if $D = 1$, then this point is $s(t)$) or on a curve or surface (if the relevant space dimension $D$ satisfies $D > 1$, then this is $\Gamma(t)$), whereas the $\Omega_\varepsilon(t)$-based reaction-term expressions rely on an interval (if $D = 1$), or on a proper area or volume (if $D > 1$).

**c)** The Stefan-heat-conduction problem is phenomenologically similar to our situation: Two 'phases' (melt and solid) are separated by a mush region, $\Omega_m(t)$, defined by

$$\text{enthalpy of ice} \;<\; \text{enthalpy of mixture} \;<\; \text{enthalpy of water.}$$

The temperature is zero in all of $\Omega_m(t)$! Only under special circumstances $\Omega_m(t)$ is a narrow strip (cf. Ref. [40]). We have not been able to see whether there are more than phenomenological analogies between the Stefan-problem and the carbonation-front-setting.

### 3.12 Related approaches

*Comprehensive* approaches for modeling concrete carbonation, i.e. continuum models incorporating transport, reaction, dissolution and precipitation, seem to become quite common (cf. Refs. [26, 28, 45, 46, 47, 53, 54, 60, 59], e.g.). Some of these authors consider $2D$-settings (Refs. [54, 60], e.g.). Related moving boundary considerations can be found in Ref. [26] (expository introduction of several moving boundary scenarios). In a different context, chemical reaction fronts have been treated in Ref. [44], e.g.

We note that in related fields (such as leaching and dissolution in concrete) moving-boundary formulations have proved to be a successful modeling tool for a long time (cf. Refs. [48, 36, 50], e.g.).

## 4 Numerical simulation of accelerated carbonation tests

### 4.1 Simulation strategy

In our simulation we will study the following questions:

1. Do the models $(P_\Gamma)$ and $(P_{\Gamma\epsilon})$ reproduce a behavior of carbonating concrete which one would expect? Examples: $\sqrt{t}$-law for penetration curves (for large $t$), relatively rapid change of concentrations in $\Omega_\epsilon$.

2. How 'stable' are the models $(P_\Gamma)$ and $(P_{\Gamma\epsilon})$, respectively? More precisely: How does a change of some of the model parameters affects the model output? Example for such parameters: Diffusion coefficient for $CO_2$(g), size of the reaction constants.

3. Can model $(P_\Gamma)$ be replaced by $(P_{\Gamma\epsilon})$ if $\epsilon$ is small? Formally: Is $(P_\Gamma)$ the limit of $(P_{\Gamma\epsilon})$ as $\epsilon \to 0$ for otherwise fixed data?

4. How stable are the models with respect to the choice of the *structure* of the reaction rates? More precisely: How does a change of $k, p$ and $q$ (cf. (3), (4)) affects the model output?

5. Are the models capable of reproducing experimental data?

Note: Question 5 is more of a academic interest, since the models $(P_\Gamma)$ and $(P_{\Gamma\epsilon})$ neglect other carbonatable phases as well as carbonation in $\Omega_1$.

## 4.2 Numerical approach to Model ($P_\Gamma$)

In this section we discuss some results obtained via numerical simulation of the equations described by the model ($P_\Gamma$) (see Remarks 3.11 a)). The major difficulty in solving the problem numerically is the moving boundary. One of the possible solutions is to transform the problem into an appropriate fixed domain formulation (for instance, cf. Ref. [14]). However, such formulations are not achieved without a trade-off which complicates the underlying pde structure by introducing additional non-linearities to compensate the fixing of the moving boundary. In this paper we use the Landau-type transformations (cf., e.g., Refs. [35, 6, 14])

$$x \in [0, s(t)] \to y = \frac{x}{s(t)} \in [0, 1]$$

and

$$x \in [s(t), L] \to y = \frac{x - s(t)}{L - s(t)} \in [0, 1]$$

to normalize the length of the carbonated layer and of the uncarbonated layer. See the reference picture Fig. 2a. Writing

$$w_i(y,t) = \bar{w}_i(x,t) - \lambda_{\bar{w}_i},\ i = 1, 2 \tag{34}$$

$$c(y,t) = \bar{c}(x,t) - \lambda_{\bar{c}}, \tag{35}$$

$$d(y,t) = \bar{d}(x,t) - \lambda_{\bar{d}}, \tag{36}$$

$$h(y,t) = \bar{h}(x,t) - \lambda_{\bar{h}}, \tag{37}$$

$$b(y,t) = \bar{b}(x,t) - \lambda_{\bar{b}}, \tag{38}$$

we obtain a system of equations on the fixed domain $0 < y < 1$. The domain becomes simpler, whereas the system becomes more complex than the original problem. The functions $w_1$, $w_2$, $c$, $h$, $b$, $d$ and $s$ are nonlinearly related. The model equations given in section 3.4 transform into

$$w_{1,t} = \frac{D_{w_1}}{s(t)^2} w_{1,yy} + \frac{\dot{s}(t)}{s(t)} y w_{1,y} + \eta_\Gamma(1,t), \tag{39}$$

$$w_{2,t} = \frac{D_{w_2}}{(L - s(t))^2} w_{2,yy} + \frac{\dot{s}(t)}{L - s(t)} (1 - y) w_{2,y}, \tag{40}$$

$$c_{,t} = \frac{D_{c_2}}{s(t)^2} c_{,yy} + \frac{\dot{s}(t)}{s(t)} y c_{,y} + P_H \left(Q_H d - c\right) + P_H \left(Q_H \lambda_{\bar{d}} - \lambda_{\bar{c}}\right), \tag{41}$$

$$d_{,t} = \frac{D_{d_1}}{s(t)^2} d_{,yy} + \frac{\dot{s}(t)}{s(t)} y d_{,y} - P_H \left(Q_H d - c\right) - P_H \left(Q_H \lambda_{\bar{d}} - \lambda_{\bar{c}}\right), \tag{42}$$

$$h_{,t} = \frac{D_{h_2}}{(L-s(t))^2} h_{,yy} + \frac{\dot{s}(t)}{L-s(t)}(1-y)h_{,y} + S_{h2diss}P_{h2diss}h, \tag{43}$$

$$b_{,t} = \frac{\dot{s}(t)}{s(t)} y b_{,y} + \eta_\Gamma(1,t), \tag{44}$$

where $\eta_\Gamma = \eta_\Gamma(y,t)$[4] denotes the reaction rate in the new variables $(y,t)$. In order to simplify the notations, we dropped the index $R$ when denoting the reaction rate. Thus, $\eta_{R\Gamma\epsilon}, \eta_{R\Gamma}$ become $\eta_{\Gamma\epsilon}, \eta_\Gamma$. The boundary and interface conditions described in sections 3.6, 3.7.1, 3.8.1 and 3.9.1 become

$$w_1(0,t) = 0, \quad -\tfrac{D_{w_1}}{s(t)} w_{1,y}(1,t) = 0, \tag{45}$$

$$w_2(1,t) = 0, \quad \tfrac{D_{w_2}}{L-s(t)} w_{2,y}(0,t) = 0, \tag{46}$$

$$c(0,t) = 0, \quad -\tfrac{D_{c_1}}{s(t)} c_{,y}(1,t) = \eta_\Gamma(1,t), \tag{47}$$

$$d(0,t) = 0, \quad -\tfrac{D_{d_1}}{s(t)} d_{,y}(1,t) = 0, \tag{48}$$

$$h(1,t) = 0, \quad \tfrac{D_{h_2}}{L-s(t)} h_{,y}(0,t) = \eta_\Gamma(0,t), \tag{49}$$

and

$$\dot{s}(t) = \frac{1}{h(1,t) + \lambda_{\bar{h}}} \eta_\Gamma(1,t), \tag{50}$$

where $t > 0$, $0 < y < 1$ and $h(1,t)$ is the concentration of $Ca(OH)_2$(aq) at $\Gamma(t)$. In the accelerated test, the carbonation process was assumed to start when a very thin layer of carbonated concrete was initially present on the surface of concrete. This layer, denoted by $\Omega_{10}$[5], was carbonated during the 5 months after the curing, when the concrete was exposed to the climatization room (at controlled humidity and temperature) with 0.03vol.% $CO_2$(g). Therefore, the concentrations of chemical species within this layer were initially taken to be $\bar{w}_i(x,0) = \bar{w}_{0i}(x) = \lambda_{\bar{w}_i}, i = 1,2$, $\bar{c}(x,0) = \bar{c}_0(x) = \lambda_{\bar{c}}$, $\bar{d}(x,0) = \bar{d}_0(x) = \lambda_{\bar{d}}$, $\bar{h}(x,0) = \bar{h}_0(x) = \lambda_{\bar{h}}$, $\bar{b}(x,0) = b_0(x) = \lambda_{\bar{b}}$. Cf. (34)-(38), we then obtain

$$w_i(y,0) = 0, i = 1,2 \tag{51}$$

$$c(y,0) = 0, \tag{52}$$

$$d(y,0) = 0, \tag{53}$$

[4]Cf. (32) and (33), $\tilde{\eta}_{R\Gamma\epsilon}$ denotes the reaction rate concentrated in $\Omega_\epsilon(t)$ depending on some concentrations, and, $\eta_{R\Gamma\epsilon}$ denotes the same reaction rate pointing out the dependence on $(x,t)$ variables. Similar considerations are made for the $\Gamma(t)$-concentrated reaction. To denote the reaction rate in the transformed domain $0 < y < 1$, $t > 0$, we used the same notation as in the case of the physical domain $0 < x < L$, $t > 0$.

[5]We assume that the layer $\Omega_{10}$ has the width $d_{10} > 0$. See also the comments in section 4.4.2.

$$h(y,0) = 0, \tag{54}$$

$$b(y,0) = 0. \tag{55}$$

Take

$$s(0) = s_0, \tag{56}$$

where $s_0 > 0$ represents the width of the initial layer.

To solve numerically the system (39)-(56), we used its weak formulation. Hence, we obtained:

$$(w_{1,t},\psi) = \frac{\dot{s}(t)}{s(t)}(yw_{1,y},\psi) - \frac{D_{w_1}}{s^2(t)}w_{1,y}(0,t)\psi(0) - \frac{D_{w_1}}{s^2(t)}(w_{1,y},\psi') + \eta_\Gamma(1,t)\psi(1), \tag{57}$$

$$(w_{2,t},\psi) = \frac{\dot{s}(t)}{L-s(t)}\left((1-y)w_{2,y},\psi\right) + \frac{D_{w_2}}{(L-s(t))^2}w_{2,y}(1,t)\psi(1) - \frac{D_{w_2}}{(L-s(t))^2}(w_{2,y},\psi'), \tag{58}$$

$$(c_{,t},\psi) = \frac{\dot{s}(t)}{s(t)}(yc_{,y},\psi) - \frac{D_{c_1}}{s^2(t)}c_{,y}(0,t)\psi(0) - \frac{D_{c_1}}{s^2(t)}(c_{,y},\psi') -$$

$$-\frac{1}{s(t)}\eta_\Gamma(1,t)\psi(1) + (P_H(Q_Hd - c),\psi) + (P_H(Q_H\lambda_{\bar{d}} - \lambda_{\bar{c}}),\psi), \tag{59}$$

$$(d_{,t},\psi) = \frac{\dot{s}(t)}{s(t)}(yd_{,y},\psi) - \frac{D_{d_1}}{s^2(t)}d_{,y}(0,t)\psi(0) - \frac{D_{d_1}}{s^2(t)}(d_{,y},\psi') -$$

$$-(P_H(Q_Hd - c),\psi) - (P_H(Q_H\lambda_{\bar{d}} - \lambda_{\bar{c}}),\psi), \tag{60}$$

$$(h_{,t},\psi) = \frac{\dot{s}(t)}{L-s(t)}\left((1-y)h_{,y},\psi\right) + \frac{D_{h_1}}{(L-s(t))^2}h_{,y}(1,t)\psi(1) - \frac{D_{h_2}}{(L-s(t))^2}(h_{,y},\psi) -$$

$$-\frac{1}{L-s(t)}\eta_\Gamma(0,t)\psi(0) + \left(S_{h2diss}P_{h2diss}h,\psi\right), \tag{61}$$

$$(b_{,t},\psi) = \frac{\dot{s}(t)}{s(t)}(yb_{,y},\psi) + \eta_\Gamma(1,t)\psi(1), \tag{62}$$

for $\psi \in H^1([0,1])$(the usual Sobolev space), where $(\cdot,\cdot)$ denotes the $L^2$-inner product in the space variable.

In order to carry out the simulation, we used a linear-spline based Galerkin scheme (cf. Refs. [49], p. 63-72, [3], p. 283-286 and [6], e.g.) to discretize the system (57)-(61). For $n = 1, 2, \ldots$, let $\{\psi_j^n\}_{j=0}^n$ denote the standard piecewise linear splines on the interval $[0, 1]$ defined with respect to the uniform mesh $[0, \frac{1}{n}, \frac{2}{n}, \ldots, 1]$. That is, for $j = 0, 1, 2, \ldots, n$

$$\psi_j^n(y) = \begin{cases} 1 - |ny - j|, & \text{if } y \in \left[\frac{j-1}{n}, \frac{j+1}{n}\right] \cap [0, 1] \\ 0, & \text{elsewhere on } [0, 1]. \end{cases}$$

We let

$$w_1^n(y,t) = \sum_{j=1}^n W_{1j}^n(t)\psi_j^n(y),\ t \geq 0,\ 0 \leq y \leq 1, \tag{63}$$

$$w_2^n(y,t) = \sum_{j=1}^n W_{2j}^n(t)\psi_j^n(y),\ t \geq 0,\ 0 \leq y \leq 1, \tag{64}$$

$$c^n(y,t) = \sum_{j=1}^n C_j^n(t)\psi_j^n(y),\ t \geq 0,\ 0 \leq y \leq 1, \tag{65}$$

$$d^n(y,t) = \sum_{j=1}^n D_j^n(t)\psi_j^n(y),\ t \geq 0,\ 0 \leq y \leq 1, \tag{66}$$

$$h^n(y,t) = \sum_{j=1}^n H_j^n(t)\psi_j^n(y),\ t \geq 0,\ 0 \leq y \leq 1, \tag{67}$$

$$b^n(y,t) = \sum_{j=1}^n B_j^n(t)\psi_j^n(y),\ t \geq 0,\ 0 \leq y \leq 1, \tag{68}$$

with

$$\begin{aligned} W_1^n(t) &= [W_{11}^n(t), W_{12}^n(t), \ldots, W_{1n}^n(t)]^T \in \mathbb{R}^n, \\ W_2^n(t) &= [W_{21}^n(t), W_{22}^n(t), \ldots, W_{2n}^n(t)]^T \in \mathbb{R}^n, \\ C^n(t) &= [C_1^n(t), C_2^n(t), \ldots, C_n^n(t)]^T \in \mathbb{R}^n, \\ D^n(t) &= [D_1^n(t), D_2^n(t), \ldots, D_n^n(t)]^T \in \mathbb{R}^n, \\ H^n(t) &= [H_1^n(t), H_2^n(t), \ldots, H_n^n(t)]^T \in \mathbb{R}^n, \\ B^n(t) &= [B_1^n(t), B_2^n(t), \ldots, B_n^n(t)]^T \in \mathbb{R}^n, \end{aligned}$$

the superscript $T$ denoting transpose.

The Galerkin equations are then given by

$$\begin{aligned} M^n \dot{W}_1^n(t) = \ & -\tfrac{D_{w_1}}{s^n(t)^2} K^n W_1^n(t) + \tfrac{\dot{s}^n(t)}{s^n(t)} L_l^n W_1^n(t) + \\ & + \left[k\left(C_n^n(t) + \lambda_{\bar{c}}\right)^p \left(H_1^n(t) + \lambda_{\bar{h}}\right)^q\right] e^n, t > 0, \end{aligned} \tag{69}$$

$$M^n\dot{W}_2^n(t) = -\frac{D_{w_2}}{(L-s^n(t))^2}K^nW_2^n(t) - \frac{\dot{s}^n(t)}{L-s^n(t)}L_r^nW_2^n(t), t>0, \tag{70}$$

$$\begin{aligned} M^n\dot{C}^n(t) = \; & -\tfrac{D_{c_1}}{s^n(t)^2}K^nC^n(t) + \tfrac{\dot{s}^n(t)}{s^n(t)}L_l^nC^n(t) - \\ & -\tfrac{1}{s^n(t)}\left[k\left(C_n^n(t)+\lambda_c\right)^p\left(H_1^n(t)+\lambda_h\right)^q\right]e^n + \\ & +P_H\left(Q_HM^nD^n(t) - M^nC^n(t)\right) + P_H\left(Q_H\lambda_{\bar{d}}^n - \lambda_{\bar{c}}^n\right), t>0, \end{aligned} \tag{71}$$

$$\begin{aligned} M^n\dot{D}^n(t) = \; & -\tfrac{D_{d_1}}{s^n(t)^2}K^nD^n(t) + \tfrac{\dot{s}^n(t)}{s^n(t)}L_l^nD^n(t) + \\ & -P_H\left(Q_HM^nD^n(t) - M^nC^n(t)\right) - P_H\left(Q_H\lambda_{\bar{d}}^n - \lambda_{\bar{c}}^n\right), t>0, \end{aligned} \tag{72}$$

$$\begin{aligned} M^n\dot{H}^n(t) = \; & -\tfrac{D_{h_2}}{(L-s^n(t))^2}K^nH^n(t) - \tfrac{\dot{s}^n(t)}{L-s^n(t)}L_r^nH^n(t) - \\ & -\tfrac{1}{L-s^n(t)}\left[k\left(C_n^n(t)+\lambda_{\bar{c}}\right)^p\left(H_1^n(t)+\lambda_{\bar{h}}\right)^q\right]e^1 + S_{h2diss}P_{h2diss}M^nH^n(t), t>0, \end{aligned} \tag{73}$$

$$M^n\dot{B}^n(t) = \frac{\dot{s}^n(t)}{s^n(t)}L_l^nB^n(t) + \left[k\left(C_n^n(t)+\lambda_{\bar{c}}\right)^p\left(H_1^n(t)+\lambda_{\bar{h}}\right)^q\right]e^n, t>0. \tag{74}$$

The initial conditions are

$$W_1^n(0) = 0, \tag{75}$$

$$W_2^n(0) = 0, \tag{76}$$

$$C^n(0) = 0, \tag{77}$$

$$D^n(0) = 0, \tag{78}$$

$$H^n(0) = 0, \tag{79}$$

$$B^n(0) = 0. \tag{80}$$

To describe the discrete interface condition we took into account the following reaction rate proportional to the product of concentration across $\Gamma(t)$:

$$\dot{s}^n(t) = \frac{1}{H_1^n(t)+\lambda_{\bar{h}}}\eta_\Gamma(t),\ t>0, \tag{81}$$

where $\eta_\Gamma(t) = k(C_n^n(t)+\lambda_{\bar{c}})^p(H_1^n(t)+\lambda_{\bar{h}})^q$ and $p, q \in [0,2]$ are the reaction orders of $CO_2$(aq) and $Ca(OH)_2$(aq), respectively. The values $C_n^n(t)$ and $H_1^n(t)$ are the corresponding amounts of $CO_2$(aq) and $Ca(OH)_2$(aq) participating to the reaction on the surface $\Gamma(t)$. For more details on surface chemical kinetics, see Ref. [2], Chapter 26, e.g.

Notice that in the simulation results we assumed the equilibrium concentrations $\lambda_i$, $i = \bar{w}_1, \bar{w}_2, \bar{c}, \bar{d}, \bar{h}, \bar{b}$, which appear in the model as Dirichlet boundary conditions, to be constant. In the present approach these concentrations (valid in $\Omega(t)$) do not differ from the corresponding initial concentrations (valid in $\Omega(0)$). See also section 3.10.

The matrices $M^n,\ K^n \in \mathbb{R}^{(n+1)\times(n+1)}$, $L_l^n,\ L_r^n \in \mathbb{R}^{n\times n}$ and $e^1, e^n, \lambda_{\bar{c}}^n, \lambda_{\bar{d}}^n \in \mathbb{R}^n$, $n \in \mathbb{N}, n > 1$ are given by

$$M^n = \frac{1}{n}\begin{bmatrix} \frac{1}{3} & \frac{1}{6} & 0 & 0 & 0 & \dots & 0 & 0 & 0 \\ \frac{1}{6} & \frac{2}{3} & \frac{1}{6} & 0 & 0 & \dots & 0 & 0 & 0 \\ 0 & \frac{1}{6} & \frac{2}{3} & \frac{1}{6} & 0 & \dots & 0 & 0 & 0 \\ 0 & 0 & \frac{1}{6} & \frac{2}{3} & \frac{1}{6} & \dots & 0 & 0 & 0 \\ \dots & \dots & \dots & \dots & \dots & \dots & \dots & \dots & \dots \\ 0 & 0 & 0 & 0 & 0 & \dots & \frac{1}{6} & \frac{2}{3} & \frac{1}{6} \\ 0 & 0 & 0 & 0 & 0 & \dots & 0 & \frac{1}{6} & \frac{1}{3} \end{bmatrix}$$

$$K^n = n\begin{bmatrix} 1 & -1 & 0 & 0 & 0 & \dots & 0 & 0 & 0 \\ -1 & 2 & -1 & 0 & 0 & \dots & 0 & 0 & 0 \\ 0 & -1 & 2 & -1 & 0 & \dots & 0 & 0 & 0 \\ 0 & 0 & -1 & 2 & -1 & \dots & 0 & 0 & 0 \\ \dots & \dots & \dots & \dots & \dots & \dots & \dots & \dots & \dots \\ 0 & 0 & 0 & 0 & 0 & \dots & -1 & 2 & -1 \\ 0 & 0 & 0 & 0 & 0 & \dots & 0 & -1 & 1 \end{bmatrix}$$

$$L_l^n = \frac{1}{n}\begin{bmatrix} -\frac{1}{3} & \frac{3i+1}{6} & 0 & 0 & \dots & 0 & 0 & 0 \\ -\left(\frac{3i-1}{6}\right) & -\frac{1}{3} & \frac{3i+1}{6} & 0 & \dots & 0 & 0 & 0 \\ \dots & \dots & \dots & \dots & \dots & \dots & \dots & \dots \\ 0 & 0 & 0 & 0 & \dots & -\left(\frac{3i-1}{6}\right) & -\frac{1}{3} & \frac{3i+1}{6} \\ 0 & 0 & 0 & 0 & \dots & 0 & -\left(\frac{3i-1}{6}\right) & \frac{3i-1}{6} \end{bmatrix}$$

$$L_r^n = \frac{1}{n}\begin{bmatrix} \frac{-6n-2}{3n} & \frac{6(i-n)-1}{3} & 0 & 0 & \dots & 0 & 0 & 0 \\ \frac{6(i-n)+1}{3} & -\frac{1}{3} & \frac{6(i-n)-1}{3} & 0 & \dots & 0 & 0 & 0 \\ \dots & \dots & \dots & \dots & \dots & \dots & \dots & \dots \\ 0 & 0 & 0 & 0 & \dots & \frac{6(i-n)+1}{3} & -\frac{1}{3} & \frac{6(i-n)-1}{3} \\ 0 & 0 & 0 & 0 & \dots & 0 & \frac{6(i-n)+1}{3} & -\frac{1}{3} \end{bmatrix}$$

$$e^n = [0,\ 0,\ \dots\ ,0,\ 1]^T, \quad e^1 = [1,\ 0,\ \dots\ ,0,\ 0]^T,$$

$$\lambda_{\bar{c}}^n = \lambda_{\bar{c}}\left[\frac{1}{n}, \frac{1}{n}, \dots, \frac{1}{n}, \frac{1}{2n}\right]^T, \quad \lambda_{\bar{d}}^n = \lambda_{\bar{d}}\left[\frac{1}{n}, \frac{1}{n}, \dots, \frac{1}{n}, \frac{1}{2n}\right]^T,$$

where

$$[M^n]_{ij} = \int_0^1 \psi_i^n(y)\psi_j^n(y)dy,\ [K^n]_{ij} = \int_0^1 \psi_i^{n\prime}(y)\psi_j^{n\prime}(y)dy,\ i,j = 1,2,\dots,n+1,$$

$$[L_l^n]_{ij} = \int_0^1 y\psi_i^n(y)\psi_j^{n\prime}(y)dy,\ [L_r^n]_{ij} = \int_0^1 (y-1)\psi_i^n(y)\psi_j^{n\prime}(y)dy,\ i,j = 1,2,\dots,n.$$

The stiffness matrix $M^n$ is sparse, symmetric, positive definite and diagonally dominant. Therefore inversion is well conditioned and straightforward. To obtain the results presented below, the initial value problem (56), (69)-(81) was integrated on a SUN ULTRA SPARC-II 5-10 using the MATLAB built-in code `ode15s` (see details in Ref. [57]) to invert a $(6n+1)\times(6n+1)$ stiff system.

## 4.3 Simulation results for $(P_\Gamma)$

The numerical results were obtained using the material parameters summarized in Table 3. These parameters and their variations were used to simulate their effects on the carbonation depth. In order to test the model using known values from literature, all of the parameters listed in Table 3 were assumed as constant throughout the concrete sample. Other assumptions on the choice of rate law might also be taken into consideration (see, for instance, Refs. [13, 45, 46, 47, 54, 59, 38]).

### 4.3.1 Standing assumptions

• No other reacting or competing species besides $CO_2$(g) and $Ca(OH)_2$(aq) contribute to the carbonation reaction. More precisely, the calcium ion liberated from the dissolution of calcium silicate hydrate ($3CaO \cdot 2SiO_2 \cdot 3H_2O$, or shortly, $CSH$) is not considered, since its solubility in alkaline environment is quite low compared with that of calcium hydroxide. This restriction implies that a few of molecules of $Ca(OH)_2$(s), which are enclosed by non-carbonated $CSH$ parts, do not react with $CO_2$(aq). Hence, we expect that, in reality, further carbonation with lower velocity might take place. In the present numerical approach we consider only the case of *complete* carbonation of $Ca(OH)_2$. This means that right behind or at the interface $\Gamma(t)$ the maximum of production of $CaCO_3$ is reached (or equivalently, the degree of carbonation attains its maximum). Since in the composition of CEM I the carbonatable reactants $K_2O$ and $Na_2O$ are present in only very small amounts (see Table 6), we neglect their contribution to $CO_2$ consumption.
• The law describing the surface reaction rate is given cf. Ref. [2], p. 787. We assume that reaction (1) is of the order $p + q$ with $p, q \in [0, 2]$.
• Hydration of concrete has been completed during the 5 months after curing. We assume that during the accelerated test no significant production by hydration appears. Therefore, the influences of the degree of hydration and porosity change due to subsequent hydration on the carbonation rate can be neglected.
• The concrete is unsaturated and sufficiently wet to permit carbonation. The inner parts of the pores are considered as filled with liquid water (namely, water in aqueous phase) and moisture (i.e. a mixture of dry air and water vapor under isobar conditions). Water molecules are considered attached to a water layer against the pore walls in the places where dissolution, precipitation and carbonation reactions happen.
• The calcium hydroxide content is considered available in solution and free to react with $CO_2$(aq). The very low solubility of the main reaction product (calcite) implies a fast precipitation of $CaCO_3$(aq) on the pore walls.
• The temperature of the reaction mixture is constant throughout the course of the accelerated test.
• The range of relative humidity in which the model given in Section 3 is applicable is $[0.4, 0.7]$. In the numerical example the concrete sample is considered in equilibrium with 0.65 relative humidity. Since we are not aware of the exact water content vs. relative humidity relationship for the concrete sample placed in the carbonation chamber, we took into account two possible (initial) values for the water content (e.g., cf. Table 6 and Fig. 18, respectively) corresponding to 0.65 RH.

### 4.3.2 Simulation results

| *Parameters tested* | *Values* | *Carb. depth after 9 weeks* |
|---|---|---|
| Reaction orders, $(p,\, q)$ | $(1,1)$ Dimensionless | 8.5 mm |
| | $(1.2, 0.8)$ | 33 |
| $(k, D_{d_1}, \alpha) = (5, 7, 2 \times 10^3)$ | $(1.1, 0.9)$ | 16 |
| Carbonation rate constant, $k$ | 5 (g cm$^{-3}$)$^{1-p-q}$ day$^{-1}$ | 16 |
| (compare to Ref. [38]) | 0.5 | 0.17 |
| $(p, q, D_{d_1}, \alpha) = (1, 1, 7, 2 \times 10^3)$ | 50 | 55 |
| Factor $\alpha$ in relation (*) below | $10^4$ Dimensionless | 2.5 |
| $(p, q, k, D_{d_1}) = (1, 1, 5, 7)$ | $2 \times 10^3$ | 16 |
| (*) $\dot{s}(t) = \frac{k\bar{c}(s(t),t)^p \bar{h}(s(t),t)^q}{\alpha \bar{h}(s(t),t)}$ | $5 \times 10^2$ | 30 |
| | $10^2$ | 96 |

Table 1: Results of robustness analysis for controlling parameters.

Several numerical experiments were done to identify the carbonation rate constant $k$, the reaction orders $(p, q)$, the diffusion coefficient $D_{d_1}$ of $CO_2$(g) and their contribution in the carbonation process. In this model (cf. 3.10), the carbonation process is assumed to begin when a very thin layer of $CaCO_3$ is initially present at the boundary of the sample.

The simulations were performed using the parameter values in Table 3. Sensitivity analyses were done with respect to the influence of the $CO_2$(g) effective diffusion coefficient on the calculated penetration depth and with respect to the carbonation rate law. The values for the effective diffusion coefficient of $CO_2$(g) given in Refs. [46] and [59] are included within the chosen numerical range (Table 3), when the inner relative humidity of the sample is 0.65. The results for varying the rate constant $k$, the reaction orders $p$, $q$ of the reactants $CO_2$(g) and $Ca(OH)_2$(aq), and also, the diffusivity $D_{d_1}$ are given in Table 1.
The results indicate a strong dependence of the penetration speed on the structure of carbonation reaction rate and on the range of effective diffusion coefficient for $CO_2$(g). It was numerically confirmed (within the ranges from Table 3) that the carbonation reaction is much faster than the diffusion of $CO_2$(g). The change in reaction orders $(p, q)$ has a lower influence on the carbonation depth than the alteration of the rate constant $k$. Increase in the diffusivity of $CO_2$(g) led to a considerable increase in the penetration depth (see Table 1). We remark that one of most important parameters is the rate constant $k$. Fig. 11 show the 'concentration vs. depth' profiles for the species involved in the carbonation process and point out their numerical range near the carbonation front. In Fig. 12 and Fig. 13 the numerical solution is compared to averaged carbonation depths measured on cross-sectioned concrete slices immediately after spraying with phenolphthalein.
The results show that the carbonation speed behaves like $t^\beta$ with $\beta$ close to $\frac{1}{2}$ as $t$ increases (as should be expected for constant humidity conditions). For small $t$, $\beta$ is close to 1. One observes that the deviation of the numerical predictions from the measurements (cf. Ref. [58]) is between $2-3$ mm and $1-2$ cm for a 9 weeks test. This shows a relatively high speed of carbonation possibly due to the fact that, in this model, only dissolved $Ca(OH)_2$ participates to the reaction (1). We expect a lower carbonation speed when all the carbonatable species react with $CO_2$.

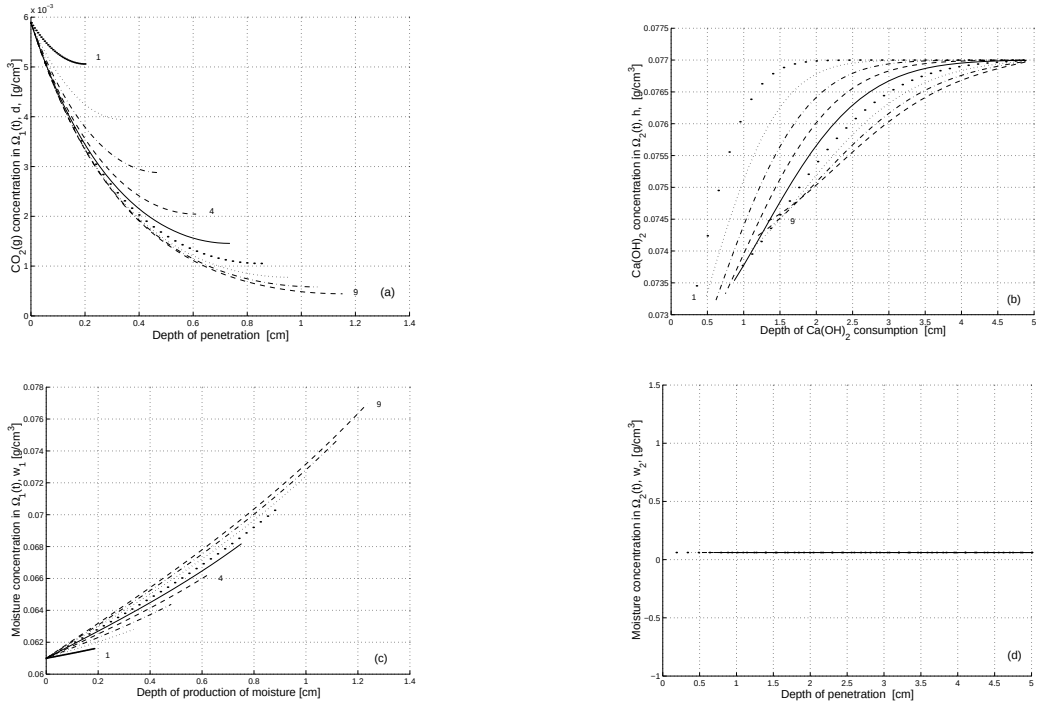


Figure 11: Simulation via $(P_\Gamma)$ model: (a) Profiles of $CO_2$(g) in $\Omega_1(t)$; (b) Profiles of $Ca(OH)_2$(aq) in $\Omega_2(t)$; (c) Moisture profiles in $\Omega_1(t)$; (d) Moisture profiles in $\Omega_2(t)$. Pictures (a) and (b) point out the consumption of $CO_2$(g) and of $Ca(OH)_2$ at the interface $\Gamma(t)$, respectively, whereas (c) and (d) show typical profiles of moisture in $\Omega_1(t)$ and $\Omega_2(t)$, respectively. The position of the moving interface between the carbonated part and uncarbonated part is indicated by the end of each curve. Plots were obtained from data at the end of each 7 days interval. $D_{d_1} = 3.5$ cm$^2$day$^{-1}$, $(p, q) = (2, 0)$ and $k = 5 \times 10^3 \left(\text{g cm}^{-3}\right)^{-1}$ day$^{-1}$. See Table 3 for other input parameters.

## 4.4 Numerical approach of Model ($P_{\Gamma\epsilon}$)

### 4.4.1 The simulation procedure

As in section 4.2, we used the following modified Landau-type transformations

$$y = \frac{x}{s(t) + \frac{\epsilon}{2}}, \text{ if } x \in [0, s(t) + \frac{\epsilon}{2}] \tag{82}$$

and

$$y = \frac{L - x}{L - s(t) + \frac{\epsilon}{2}}, \text{ if } x \in [s(t) - \frac{\epsilon}{2}, L] \tag{83}$$

to transform the moving regions $\Omega_1(t) \cup \Omega_\epsilon(t)$ and $\Omega_2(t) \cup \Omega_\epsilon(t)$ into fixed ones. In $\Omega_1(t) \cup \Omega_\epsilon(t)$, $0 \leq x \leq s(t) + \frac{\epsilon}{2}$, the moving $\Gamma_r(t)$ is fixed so that $x = 0$ becomes $y = 0$ and $x = s(t) + \frac{\epsilon}{2}$ is $y = 1$. In $\Omega_2(t) \cup \Omega_\epsilon(t)$, $s(t) - \frac{\epsilon}{2} \leq x \leq L$, the moving $\Gamma_l(t)$ is fixed so that $x = s(t) - \frac{\epsilon}{2}$ becomes $y = 1$ and $x = L$ is $y = 0$. Denoting

$$l_{1\epsilon} = 1 - \frac{\epsilon}{s(t) + \frac{\epsilon}{2}},$$

and

$$l_{2\epsilon} := 1 - \frac{\epsilon}{L - s(t) + \frac{\epsilon}{2}},$$

we notice that the layer $\Omega_\epsilon(t)$ transforms successively into $[l_{1\epsilon}, 1]$ and $[l_{2\epsilon}, 1]$, respectively (cf. (82), and then, cf. (83)).

Introducing the homogenized concentrations

$$c(y,t) = \bar{c}(x,t) - \lambda_{\bar{c}}, \tag{84}$$

$$d(y,t) = \bar{d}(x,t) - \lambda_{\bar{d}}, \tag{85}$$

$$h(y,t) = \bar{h}(x,t) - \lambda_{\bar{h}}, \tag{86}$$

$$b(y,t) = \bar{b}(x,t) - \lambda_{\bar{b}}, \tag{87}$$

and using the transformations (82) and (83), we obtain a system of equations on the fixed domain $0 < y < 1$. According to (82) and (83), the pde's in model ($P_{\Gamma\epsilon}$) (defined in section 3.11) transform into:

$$c_{,t} = \frac{D_{c_2}}{\left(s(t) + \frac{\epsilon}{2}\right)^2} c_{,yy} + \frac{\dot{s}(t)}{s(t) + \frac{\epsilon}{2}} y c_{,y} + f_{\bar{c}Henry} + f_{\bar{c}reac}, \tag{88}$$

$$d_{,t} = \frac{D_{d_1}}{\left(s(t) + \frac{\epsilon}{2}\right)^2} d_{,yy} + \frac{\dot{s}(t)}{s(t) + \frac{\epsilon}{2}} y d_{,y} + f_{\bar{d}Henry}, \tag{89}$$

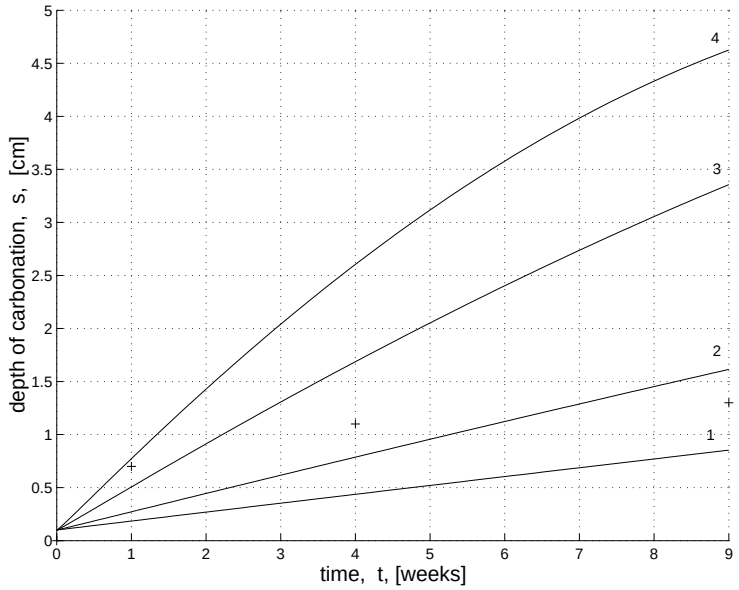


Figure 12: Carbonation penetration (in cm) after 9 weeks of accelerated testing (simulation via $(P_\Gamma)$ model). The graphs were obtained varying $(p, q) = (1, 1), (1.1, 0.9), (1.2, 0.8), (1.25, 0.75)$, when $(k, D_{d_1}, \alpha) = (5, 7, 2 \times 10^3)$ are kept fixed. The penetration depths after 9 weeks shown in plots 3 and 4 (here and in Fig. 13) are twice as high as in the ace test. '+' denotes experimental values.

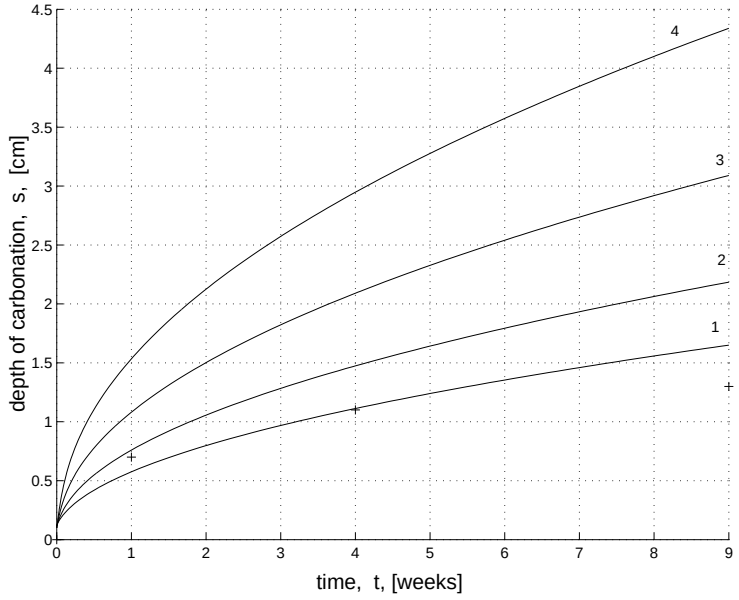


Figure 13: Carbonation penetration (in cm) after 9 weeks of accelerated testing (simulation via $(P_\Gamma)$ model). The graphs were obtained varying the $CO_2$(g) diffusivity $D_{d_1} = 1, \frac{7}{4}, \frac{7}{2}, 7$(cf. Ref. [59]), when $(p, q, k, \alpha) = (1, 1, 5 \times 10^3$(cf. Ref. [38]), 10) are kept fixed and $\lambda_{\bar{d}} = 58.92 \times 10^{-4}$ g cm$^{-3}$. '+' denotes experimental values.

$$h_{,t} = \frac{D_{h_2}}{\left(s(t) - \frac{\epsilon}{2} - L\right)^2} h_{,yy} + \frac{\dot{s}(t)}{s(t) - \frac{\epsilon}{2} - L} y h_{,y} + f_{\bar{h}2diss} + f_{\bar{h}reac}, \tag{90}$$

$$b_{,t} = \frac{\dot{s}(t)}{s(t) + \frac{\epsilon}{2}} y b_{,y} + f_{\bar{b}_w reac}. \tag{91}$$

Note: For the case of non-constant diffusion coefficients one obtains a slightly different system of pde's.

The boundary conditions associated with the model $(P_{\Gamma\epsilon})$ (cf. section 3.7.2) become

$$c(0,t) = 0, \quad -\frac{D_{c_1}}{s(t)+\frac{\epsilon}{2}} c_{,y}(1,t) = \dot{s}\,(t)\,(c(1,t) + \lambda_{\bar{c}})\,, \tag{92}$$

$$d(0,t) = 0, \quad -\frac{D_{d_1}}{s(t)+\frac{\epsilon}{2}} d_{,y}(1,t) = \dot{s}\,(t)\,(d\,(1,t) + \lambda_{\bar{d}})\,, \tag{93}$$

$$h(0,t) = 0, \quad \frac{D_{h_2}}{s(t)-\frac{\epsilon}{2}-L} h_{,y}(1,t) = -\dot{s}\,(t)\,(h(1,t) + \lambda_{\bar{h}}) \tag{94}$$

and the relation defining the speed of the layer $\Omega_\epsilon(t)$ (cf. section 3.9), reads as

$$\dot{s}(t) = \frac{\int_{\Omega_\epsilon(t)} \bar{\eta}_{\Gamma\epsilon}(x,t)dx}{\frac{1}{\epsilon}\int_{\Omega_\epsilon(t)} (h(x,t) + \lambda_{\bar{h}})\,dx}, \tag{95}$$

where $t > 0$ and $0 < y < 1$.

We keep the same initial conditions and uniform mesh as in section 4.2.

The *weak formulation* of the transformed problem (88)-(95) together with the Galerkin ansatz (65) - (68) lead to the following system of ode's:

$$\begin{aligned} M^n \dot{C}^n(t) = \; & -\frac{D_{c_1}}{\left(s^n(t)+\frac{\epsilon}{2}\right)^2} K^n C^n(t) + \frac{\dot{s}^n(t)}{s^n(t)+\frac{\epsilon}{2}} L_l^n C^n(t) - \\ & -\frac{\dot{s}^n(t)}{s^n(t)+\frac{\epsilon}{2}} \left(C_n^n(t) + \lambda_{\bar{c}}\right) e^n + \\ & + P_H \left(Q_H M^n D^n(t) - M^n C^n(t)\right) + P_H \left(Q_H \lambda_{\bar{d}}^n - \lambda_{\bar{c}}^n\right) + f_{\bar{c}reac}^n, \; t > 0, \end{aligned} \tag{96}$$

$$\begin{aligned} M^n \dot{D}^n(t) = \; & -\frac{D_{d_1}}{\left(s^n(t)+\frac{\epsilon}{2}\right)^2} K^n D^n(t) + \frac{\dot{s}^n(t)}{s^n(t)+\frac{\epsilon}{2}} L_l^n D^n(t) - \\ & -\frac{\dot{s}^n(t)}{s(t)+\frac{\epsilon}{2}} \left(D_n^n(t) + \lambda_{\bar{d}}\right) e^n - \\ & - P_H \left(Q_H M^n D^n(t) - M^n C^n(t)\right) - P_H \left(Q_H \lambda_{\bar{d}}^n - \lambda_{\bar{c}}^n\right), \; t > 0, \end{aligned} \tag{97}$$

$$\begin{aligned} M^n \dot{H}^n(t) = \; & -\frac{D_{h_2}}{(s^n(t)-\frac{\epsilon}{2}-L)^2} K^n H^n(t) + \frac{\dot{s}^n(t)}{s^n(t)-\frac{\epsilon}{2}-L} L_l^n H^n(t) - \\ & -\frac{\dot{s}^n(t)}{s^n(t)-\frac{\epsilon}{2}-L} \left(H_n^n(t) + \lambda_{\bar{h}}\right) e^n + \\ & + S_{h2diss} P_{h2diss} M^n H^n(t) + f_{\bar{h}reac}^n, \; t > 0, \end{aligned} \tag{98}$$

$$M^n\dot{B}^n(t) = \frac{\dot{s}^n(t)}{s^n(t)+\frac{\epsilon}{2}} L_l^n B^n(t) + f_{\bar{b}reac}^n,\ t>0, \tag{99}$$

where the discrete production terms are given by

$$f_{\bar{c}reac}^n = -f_{\bar{b}reac}^n = -\frac{k}{s^n(t)+\frac{\epsilon}{2}} \sum_{j=1}^{n} \int_{l_{1\epsilon}}^{1} \left(c^n(y,t)+\lambda_{\bar{c}}\right)^p \left(h^n(y,t)+\lambda_{\bar{h}}\right)^q \psi_j^n(y)dy \tag{100}$$

and

$$f_{\bar{h}reac}^n = -\frac{k}{L-s^n(t)+\frac{\epsilon}{2}} \sum_{j=1}^{n} \int_{l_{2\epsilon}}^{1} \left(c^n(y,t)+\lambda_{\bar{c}}\right)^p \left(h^n(y,t)+\lambda_{\bar{h}}\right)^q \psi_j^n(y)dy. \tag{101}$$

The initial conditions are

$$C^n(0) = 0, \tag{102}$$

$$D^n(0) = 0, \tag{103}$$

$$H^n(0) = 0, \tag{104}$$

$$B^n(0) = 0. \tag{105}$$

We approximate (95) with (106), where the right-hand side of (95) was transformed by means of (65) and (67):

$$\dot{s}^n(t) = \epsilon \frac{I_{\eta\Gamma\epsilon}^n(t)}{I_{\bar{h}\epsilon}^n(t)}. \tag{106}$$

We keep

$$s^n(0) = s_0. \tag{107}$$

The following trapezoidal rules were used to compute the integrals in the right-hand side of (106):

$$\begin{aligned} I_{\eta\Gamma\epsilon}^n(t) = \ & \frac{k\epsilon}{s^n(t)+\frac{\epsilon}{2}} [\frac{1}{2}\left(C_{n_{1\epsilon}}^n(t)+\lambda_{\bar{c}}\right)^p \left(H_{n_{1\epsilon}}^n(t)+\lambda_{\bar{h}}\right)^q + \\ & + \sum_{j=n_{1\epsilon}+1}^{n-1} \left(C_j^n(t)+\lambda_{\bar{c}}\right)^p \left(H_j^n(t)+\lambda_{\bar{h}}\right)^q + \frac{1}{2}\left(C_n^n(t)+\lambda_{\bar{c}}\right)^p \left(H_n^n(t)+\lambda_{\bar{h}}\right)^q], t>0, \end{aligned} \tag{108}$$

and

$$I_{\bar{h}\epsilon}^n(t) = \frac{\epsilon}{L-s^n(t)+\frac{\epsilon}{2}} \left(\lambda_{\bar{h}} + \frac{H_{n_{2\epsilon}}^n(t)}{2} + \sum_{j=n_{2\epsilon}+1}^{n-1} H_j^n(t) + \frac{H_n^n(t)}{2}\right), t>0, \tag{109}$$

where $n_{1\epsilon} = n - \left[\frac{n\epsilon}{6\left(s_0+\frac{\epsilon}{2}\right)}\right] - 1$ and $n_{2\epsilon} = n - \left[\frac{n\epsilon}{6\left(L-s_0+\frac{\epsilon}{2}\right)}\right] - 1$, while the width of $\Omega_\epsilon(t)$ is considered constant. It is worth mentioning that the expressions listed above approximate 'sufficiently well' $\dot{s}^n(t)$. A similar approach was adopted to calculate the production terms by reaction (100) and (101). Within this approach we consider $s_0 = d_{10} + \frac{\epsilon}{2}$, where $d_{10} > 0$ represents the width of the initial layer $\Omega_1(0) = \Omega_{10}$. In calculations we chose $d_{10} = 10^{-3}$.

With the initial concentrations set as in (102)-(105) and also (107), the resulting initial value problem was integrated using a standard variable step-size numerical ode integration scheme. We used, as in sections 4.2 and 4.3, the MATLAB routine `ode15s`.

### 4.4.2 Simulation results

This section contains the numerical experiments done for the $(P_{\Gamma\epsilon})$ model. We aim a comparison between the penetration depths obtained in the moving-interface approach $(P_\Gamma)$ and those obtained in the present moving-layer setting $(P_{\Gamma\epsilon})$. The input-data configuration used in 4.4.2 is given in the appendix.

We make the same standing modeling assumptions as in section 4.2. Additionally, in this numerical approach the humidity has the role of a parameter. Calcium carbonate concentration in the initial layer $\Omega_{10}$ is assumed to be $10^{-4}$ gcm$^{-3}$.

In simulating numerically the $(P_{\Gamma\epsilon})$ model, the qualitative behavior of the profiles of concentration near the carbonation front obtained in $(P_\Gamma)$ model has been observed again. See, e.g., Fig. 15. In Fig. 14 and in Fig. 16 - 17 one may see the change in penetration depth when varying[6] successively the parameters $D_{d_1}$, $p$, $q$, $k$, $\epsilon$. If not otherwise mentioned, $n = 100$.

We varied the effective diffusion coefficient, $D_{d_1}$, of $CO_2$(g). The results are shown in Fig. 16 where we plot the layer position as a function of time. Increasing $D_{d_1}$ we note faster penetration. This phenomenon persists also if one chooses different widths $\epsilon$. As expected (cf. the experiments done for the model $(P_\Gamma)$ in Fig. 13, and also, cf. Ref. [32], e.g.) the penetration depths (and hence, the layer position) exhibit a near square-root behavior with time. Moreover, the 'square-root shape' of the curve 'penetration depth vs. time' seems to be more stable here as in the sharp-interface model. Slight changes in the exponents $p, q$ lead to the same shape of the plots 'layer position as a function of time'. However, cf. Fig. 14 smaller values for $p$ produced lower carbonation depths, whereas bigger variations of $q$ did not affect drastically the penetration depths. Changing the reaction-rate constant $k$ by a factor of $\frac{1}{10}$ or $\frac{1}{100}$ implies that the position $s(t)$ would reach $L$ after 9 weeks of accelerated exposure.

Within the frame of the $(P_{\Gamma\epsilon})$ model, we looked specially for some information about the influence of the size of $\Omega_\epsilon(t)$ (the moving carbonation layer) on the penetration depth. Therefore, cf. Fig. 17, e.g., we found that, for smaller values of the width $\epsilon$ the precision of prediction seems to increase. If the layer's width $\epsilon$ is large, then the mesh may be coarsened, and thus, the calculations are usually faster. If $\epsilon = L$, then the boundary conditions need further discussions.

The production term by (non)-instantaneous dissolution, $f_{\bar{h}2diss}$, had no significant influence on the penetration depth. However, the exchange terms by Henry's law, $f_{\bar{c}Henry}, f_{\bar{d}Henry}$, influenced drastically the speed of carbonation (thus, to obtain Fig. 14 - 17 we used a reduced mass transfer factor $k_T \frac{A_s}{\phi_a} \approx 7$ day$^{-1}$). The production terms by reaction, $f_{\bar{c}reac}$, $f_{\bar{h}reac}$ and $f_{\bar{b}reac}$, change their influence on the penetration depth in the same time with the modification of $\epsilon$, and therefore, cf. Fig. 17 for smaller values of the width $\epsilon$ the precision of prediction seems to increase, i.e. the calculated $s(t)$ is closer to the measured one.

The results indicate, as in the case of model $(P_\Gamma)$, strong influences of the structure of the carbonation reaction rate and of the range of effective diffusion coefficient of $CO_2$(g) on the carbonation depth.

The whole model is stable with respect to small changes of $\epsilon$.

[6]Each numerical experiment represents the variation of one parameter while the other parameters and the input-data configuration are kept constant.

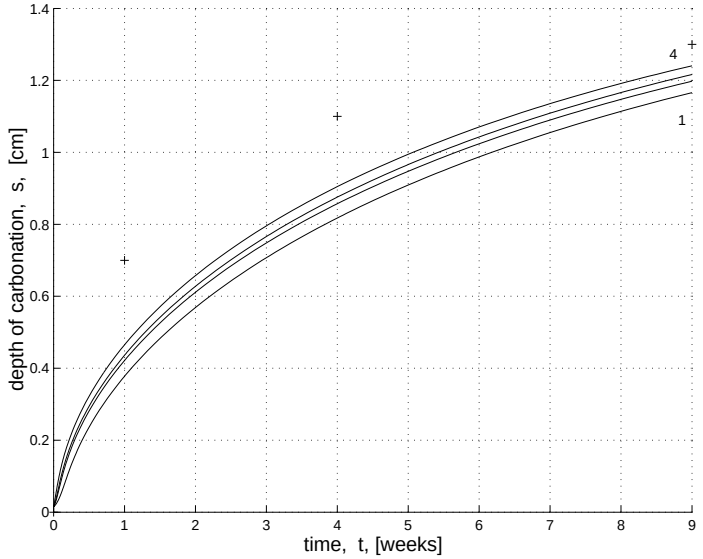


Figure 14: Carbonation penetration (in cm) after 9 weeks of accelerated testing (simulation via $(P_{\Gamma\epsilon})$ model). The graphs were obtained varying $(p,q) = (2,0)$, $(1.9,0.4)$, $(1.7,0.3)$, $(1,1)$, $(1.3,1)$, when $(\epsilon, k, D_{d_1}, \alpha) = (\frac{1}{150}, 5 \times 10^3$(cf. Ref. [38]$), 3.5$ (cf. Ref. [59]$), 10^3$(cf. (106)) are kept fixed. '+' denotes experimental values.

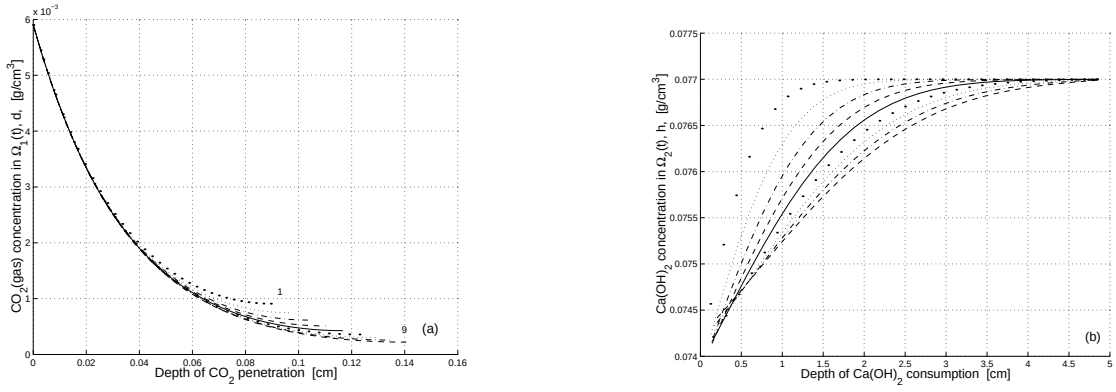


Figure 15: Simulation via $(P_{\Gamma\epsilon})$ model. (a) profiles of $CO_2$(g) in $\Omega_1(t) \cup \Omega_\epsilon(t)$ (at left side) and (b) profiles of $Ca(OH)_2$(aq) in $\Omega_2(t) \cup \Omega_\epsilon(t)$ (at right side). In (a) one notes the consumption of $CO_2$(g), whereas in (b) one observes the consumption of $Ca(OH)_2$(aq). The plots were obtained from data at the end of each 7-days interval. The position of the moving layer between the carbonated part and the uncarbonated part is indicated by the end of each curve. $(D_{d_1}, k, \alpha, p, q, \epsilon) = (3.5, 5 \times 10^3, 1, 1.8, 0.8, \frac{1}{100})$.

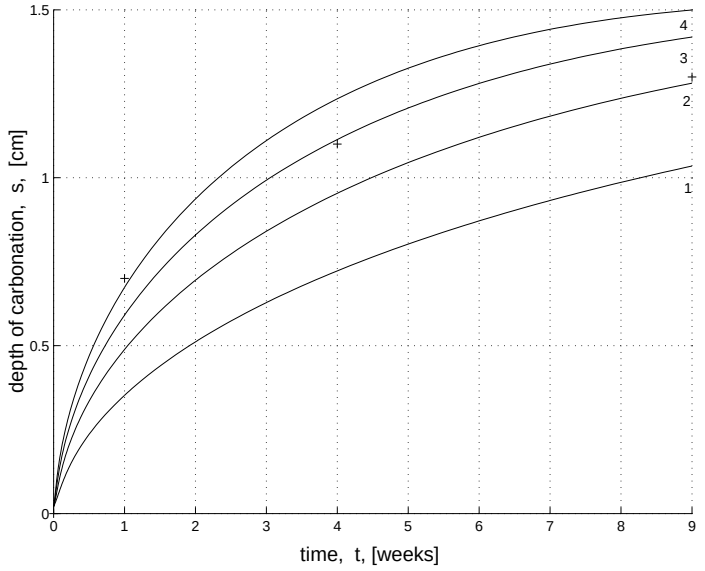


Figure 16: Carbonation penetration (in cm) after 9 weeks of accelerated testing (simulation via $(P_{\Gamma\epsilon})$ model). The graphs were obtained varying the effective diffusivity of $CO_2$(g) $D_{d_1} = \frac{7}{2}, 7, \frac{21}{2}, 14$. $(\epsilon, p, q, k, \alpha) = (\frac{1}{100}, 1.7, 0.4, 5 \times 10^3,\ 10^3)$ are kept fixed. '+' denotes experimental values.

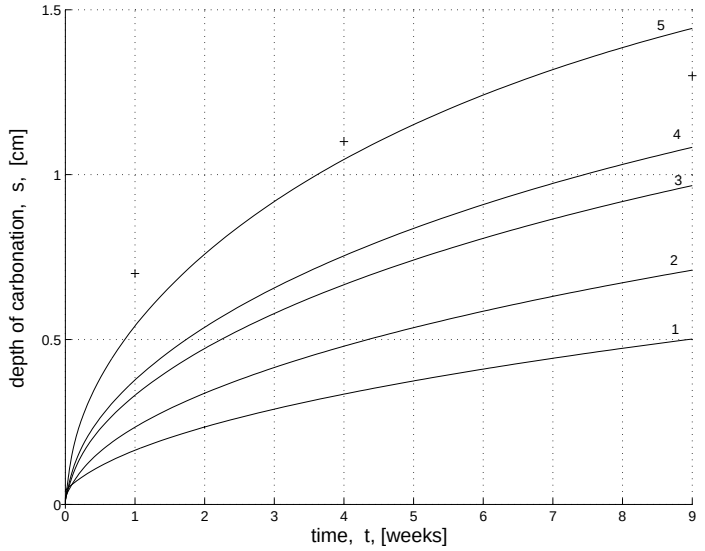


Figure 17: Carbonation penetration (in cm) after 9 weeks of accelerated testing (simulation via $(P_{\Gamma\epsilon})$ model). The graphs were obtained varying the width $\epsilon = \frac{1}{50}, \frac{1}{100}, \frac{1}{200}, \frac{1}{250}, \frac{1}{500}$ when $n = 200$ and $(k, D_{d_1}, p, q, \alpha) = (5 \times 10^3, 3.5, 1, 1, 10^3)$ are kept fixed. Comparing the graphs from bottom to top one notes that smaller $\epsilon$ imply higher penetration speeds $\dot{s}(t)$. '+' denotes experimental values.

## 4.5 Interpretations of the numerical experiments

In this study, a moving boundary model [for each of the two scenarios $(P_\Gamma)$ and $(P_{\Gamma_\epsilon})$], for the prediction of carbonation-penetration depth of concrete exposed to $CO_2$(g) was developed. The effects of several parameters on the carbonation rate were simulated. These included effective diffusivity of $CO_2$(g), carbonation rate constant and the structure of the reaction rates.

The position of the carbonation front (sharp interface or layer) is obtained solving a moving boundary problem. The concentrations of $CO_2$(g) and $Ca(OH)_2$(aq) are calculated near the reaction front. The following conclusions can be drawn:
• Fig. 11 (a), (b) show typical concentration profiles of $CO_2$(g), $CO_2$(aq) and $Ca(OH)_2$(aq) during accelerated carbonation. They are in agreement with the profiles given by Brieger and Wittmann (Fig. 4 in Ref. [26], p. 640), and by Papadakis et al (Fig. 5 in Ref. [45], p. 1645). The numerical prediction of the position of the carbonation front is relatively close to the depth of carbonation measured by means of phenolphthalein by Sisomphon and Franke, Ref. [18], for CEM I and $w/c = 0.60$ (7 days curing). Similar results were obtained by Ishida and Maekawa (see Fig. 8 and Fig. 9 in Ref. [29], and also, Fig. 11 and Fig. 12 in Ref. [38], e.g.) without considering explicitly the sharp-interface model.
• Modifications of the reaction constant $k$ and of the reaction orders $p, q$ showed drastic changes in the evolution of carbonation and in the square-root behavior of the front's penetration. The square-root shape of the curve 'carbonation depth vs. time' may be obtained or lost by varying these reaction orders, when the effective diffusivity of $CO_2$(g) and the rate constant are kept constant.
• In the $(P_\Gamma)$ model the wetness is coupled with the other variables only by the presence of the production term $f_{\bar{w}_1 reac}$ (i.e. production of water by reaction (1)). Fig. 11 (c) and (d) point out that, based on the model discussed here, only a relatively small amount of water is produced by the carbonation reaction. Therefore the two reaction-diffusion equations describing the moisture behavior in $\Omega_1(t)$ and $\Omega_2(t)$ can be neglected within this model without harming neither the calculation of penetration depth $s$, nor the evaluation of $\bar{c}$, $\bar{d}$, $\bar{h}$ and $\bar{b}$ near the interface. Therefore, in the moving-layer setting we considered that the humidity has the role of a parameter [strongly influencing the diffusion coefficient of $CO_2$(g), for instance (cf. [45, 47], e.g.)].
• It was numerically observed that, in the $(P_\Gamma)$ model, the production term by (non)-instantaneous dissolution, $f_{\bar{h}2diss}$, and also, the production terms by Henry's law, $f_{\bar{d}Henry}$ and $f_{\bar{c}Henry}$, do not affect essentially the qualitative behavior of the profiles of $CO_2$(g) and $Ca(OH)_2$(aq) near the interface $\Gamma(t)$. A different situation appears in the $(P_{\Gamma_\epsilon})$ setting where the terms $f_{\bar{d}Henry}$ and $f_{\bar{c}Henry}$ influence significantly the carbonation speed, and hence, the penetration depth.

The numerical values of many of the model parameters (effective diffusivities, tortuosity in $\Omega_1(t)$, carbonation rate constant etc.) and their correlation with the material properties (type of cement, water/cement ratio, degree of hydration, curing time, dependence of porosity on carbonation rate etc.) are only poorly known.

Despite of the mentioned drawbacks (difficulty to obtain real data, standing model restrictions, and so on), the moving boundary approach provides a good framework for further investigation of reaction influence on overall carbonation process. We expect that better experimental data (e.g., pore size distributions, water content/relative humidity relationship, $D_{d_1}$, investigation of free calcium hydroxide content in the proximity of the observed

front, mass-transfer coefficients etc.) will simplify the system of equations, and hence, the numerical model will become more reliable and effective. This way of modeling can be adapted to various experimental settings.

# 5 Conclusions

## 5.1 Re. questions in 4.1

1. Re. question 1:

   - $(P_\Gamma)$: In Fig. 12 and Fig. 13 the penetration curve exhibits a near-$\sqrt{t}$-type behavior for large times. Note: In the context of ace 9 weeks represents large time!
     A large concentration gradient for $Ca(OH)_2$ in $\Omega_2(t)$ can be observed near $\Gamma(t)$ (cf. Fig. 11 (b)).
   - $(P_{\Gamma\epsilon})$: Near-$\sqrt{t}$-type behavior as above (cf. Fig. 14, Fig. 16 and Fig. 17).
     The concentration of $Ca(OH)_2$ in $\Omega_2(t) \cup \Omega_\epsilon(t)$ decreases rapidly near the reaction layer $\Omega_\epsilon(t)$ (see Fig. 15 (b)).

2. Re. question 2:

   - $(P_\Gamma)$: Increasing the diffusion coefficient of $CO_2$(g) or the rate constant $k$, we note faster penetration speeds (see Fig. 13 and Table 1). Small increase of $k$ imply large changes in the penetration speed.
   - $(P_{\Gamma\epsilon})$: Relatively small increase in the diffusivity of $CO_2$(g) leads to a considerable increase in the penetration depth (see Fig. 16).

3. Re. question 3:

   - If the reaction rate in $(P_{\Gamma\epsilon})$, $\eta_{\Gamma\epsilon}$, and the one in $(P_\Gamma)$, $\eta_\Gamma$, are related by $\epsilon\eta_{\Gamma\epsilon} = \eta_\Gamma$ (cf. (6)), then the model output for $(P_{\Gamma\epsilon})$ is close to the one for $(P_\Gamma)$.
     Smaller $\epsilon$ imply higher penetration speeds (see Fig. 17).

4. Re. question 4:

   - $(P_\Gamma)$: The penetration speed curve strongly depends on the structure of carbonation rate (see Fig. 12). Note: Fig. 12 shows examples of penetration curves being far from $\sqrt{t}$-like behavior.
   - $(P_{\Gamma\epsilon})$: Not so small changes in $p$ and $q$ lead to a drastic change of the penetration depth curves (see Fig. 12). Higher values for $p$ produce higher carbonation speeds, whereas larger variations of $q$ do not affect drastically the penetration speeds.

5. Re. question 5:

   - Both models $(P_\Gamma)$ and $(P_{\Gamma\epsilon})$ are capable to reproduce experimental data. See, e.g., Fig. 13 (plot 1), Fig. 14, Fig. 16 and Fig. 17 (plot 5), where the experimental values are given cf. the ace in Ref. [58].

## 5.2 General evaluation

The model is capable to reflect the major characteristics of the carbonation process such as shape and order of magnitude of the concentrations and their curves, high sensitivity with respect to the diffusion coefficient for $CO_2$, and dominance of the reaction speed against transport, e.g. Moreover the simulations indicate a strong dependence on the choice of the reaction kinetics. The model allows some freedom in the choice (for numerical simulations) of the location of the carbonation reaction - it does not matter very much whether the reaction is assumed to happen entirely on the interface $\Gamma(t)$ or in a small strip around that interface.

At the current modeling stage quantitative deviations from measurements are attributed to the neglection of other carbonatable phases such as $CSH$ and to the assumption that the carbonation reaction is restricted to $\Gamma(t)$ or to a neighboring strip $\Omega_\epsilon(t)$.

# 6 Appendix

| *Quantity* | *Definition* | *Dimensions* | *Value* |
|---|---|---|---|
| $w/c$ | Water:cement ratio | - | 0.60 |
| $a/c$ | Aggregate:cement ratio | - | 5.1429 |
| $\rho_c$ | Cement density, Refs. [58, 24] | g cm$^{-3}$ | 3.15 |
| $\rho_a$ | Aggregate density, Ref. [58] | g cm$^{-3}$ | 2.7 |
| $\rho_{H_2O}$ | Water density, Refs. [58, 24] | g cm$^{-3}$ | 1 |
| $\rho_{cp}$ | Cement paste density (CEM I 0.60), Ref. [58] | g cm$^{-3}$ | 1.7439 |
| $\rho_{CaO}$ | Calcium oxide density, Ref. [16] | g cm$^{-3}$ | 3.34 |

Table 2: Material characteristics of the concrete sample.

| *Quantity* | *Definition* | *Dimensions* | *Value/range*[a] |
|---|---|---|---|
| $D_{w_1}, D_{w_2}$ | Effective moisture diffusivities, Refs. [59, 33] | $\text{cm}^2\ \text{day}^{-1}$ | $[0.9, 90]$ |
| $D_{h_2}$ | Effective $Ca(OH)_2$(aq) diffusivity, Ref. [45] | $\text{cm}^2\ \text{day}^{-1}$ | 0.864 |
| $D_{c_1}$ | Effective $CO_2$(aq) diffusivity, Ref. [13] | $\text{cm}^2\ \text{day}^{-1}$ | $[0.62, 6.2]$ |
| $\lambda_{\bar{w}_i}$ | Initial values of moisture $i = 1, 2$, Fig. 18 and Table 6 | $\text{g cm}^{-3}$ | $[0.061, 0.123]$ |
| $\lambda_{\bar{d}}$ | Initial concentration of $CO_2$(g), Ref. [58] | $\text{g cm}^{-3}$ | $58.92 \times 10^{-4}$ |
| $\lambda_{\bar{b}}$ | Initial value for $CaCO_3$ | $\text{g cm}^{-3}$ | 0 |
| $\lambda_{\bar{h}}$ | Initial value for $Ca(OH)_2$(aq), Ref. [33] | $\text{g cm}^{-3}$ | $77.5 \times 10^{-3}$ |
| $s_0$ | Initial position of reaction front in $(P_\Gamma)$ model[b] | cm | $10^{-5}$ |
| $2L$ | Length of the observed slab, Ref. [58] | cm | 10 |
| $\phi_1$ | Porosity of non-carbonated concrete, Ref. [33] | - | 0.15 |
| $\phi_2$ | Porosity of carbonated concrete, Ref. [33] | - | 0.13 |
| $Q_H$ | Exchange term in Henry's law, Refs. [45, 6] | - | 0.8227 |
| $P_H$ | Mass transfer coefficient of $CO_2$(g) in pore water, Ref. [6] | $\text{day}^{-1}$ | 35760 |
| $P_{\bar{h}kdiss}$ | Factor in the dissolution law, $k = 1, \epsilon, 2$ | $\text{day}^{-1}$ | $\frac{1}{150}$ |
| $k_T$ | Mass transfer constant of $CO_2$(g), air to water, Ref. [6] | $\text{cm day}^{-1}$ | 7 |
| $\frac{A_s}{\phi_a}$ | Surface area to volume ratio, for air, Ref. [6] | $\text{cm}^{-1}$ | $10^4$ |
| $\frac{A_s}{\phi_w}$ | Surface area to volume ratio, for water, Ref. [6] | $\text{cm}^{-1}$ | $10^4$ |

Table 3: Numerical data for several parameters and input variables.

[a]The threshold values introduced in this table are taken from literature (cf. section 6). We use numerical ranges and not precise values since we are not aware of measurements for these parameters within the ace described in section 1.4

[b]In the $(P_{\Gamma\epsilon})$ model $s_o$ has the meaning described in section 4.4.2.

| *Quantity* | *Definition* | *Dimensions* | *Value* |
|---|---|---|---|
| $R$ | Gas constant, Ref. [16] | $\text{mol}^{-1}\ \text{K}^{-1}\ \text{atm}$ | $8206 \times 10^{-5}$ |
| $H$ | Henry's law constant for $CO_2$(g), Ref. [46] | $\text{mol m}^{-3}\text{atm}^{-1}$ | 34.2 |
| $M_{H_2O}$ | Molecular weight of water, Ref. [16] | $\text{g mol}^{-1}$ | 18 |
| $M_{CO_2}$ | Molecular weight of $CO_2$, Ref. [16] | $\text{g mol}^{-1}$ | 44 |
| $M_{CaCO_3}$ | Molecular weight of aragonite/calcite, Ref. [16] | $\text{g mol}^{-1}$ | 100.087 |
| $M_{Ca(OH)_2}$ | Molecular weight of $Ca(OH)_2$, Ref. [16] | $\text{g mol}^{-1}$ | 74 |
| $\rho_{Ca(OH)_2}$ | Density of $Ca(OH)_2$, Ref. [16] | $\text{g cm}^{-3}$ | 2.24 |
| $\rho_{CaCO_3}$ | Density of $CaCO_3$ (calcite), Ref. [16] | $\text{g cm}^{-3}$ | 2.71 |

Table 4: Useful physical and material constants.

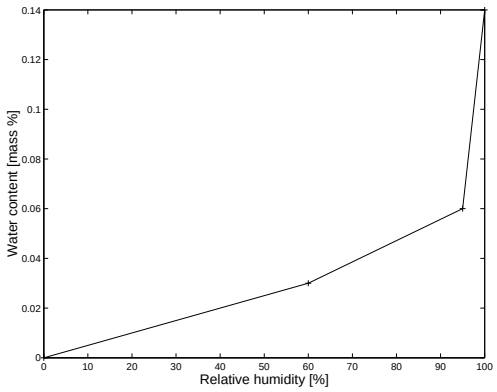


Figure 18: Sorption isotherm, cf. Ref. [23].

| Portland cement (CEM I) | |
|---|---|
| $SiO_2$ | 20 |
| $Al_2O_3$ | 6 |
| $Fe_2O_3$ | 3 |
| $CaO$ | 63 |
| $MgO$ | 1.5 |
| $SO_3$ | 2 |
| $Na_2O$ and $K_2O$ | 1 |
| Others | 1 |
| Loss on ignition | 2 |
| Insoluble residue | 0.5 |

Table 5: Composition (mass fraction %), cf. Ref. [42].

| RH (%) | $\bar{w}$ (kg/m$^3$) |
|---|---|
| 0 | 0 |
| 50 | 42 |
| 60 | 54 |
| 70 | 68 |
| 80 | 84 |
| 90 | 110 |
| 93 | 120 |
| 95 | 130 |

Table 6: Material data for concrete showing the relation between relative humidity RH and moisture content $\bar{w}$, cf. Ref. [1], III-4 . See also Fig. 4 in Ref. [27].

# References


[1] J. Arfvidsson, Moisture transport in porous media. Modeling based on Kirchhoff potentials. Ph.D. Thesis, Lund Institute of Technology, 1998.

[2] P. W. Atkins, *Physical Chemistry*. Oxford University Press, Oxford, 1990.

[3] K. Atkinson, W. Han, *Theoretical Numerical Analysis. A Functional Analysis Framework*. Springer Verlag, Berlin, 2001.

[4] R. E. Beddoe, Private communications, (2002).

[5] M. Böhm, *Lecture Notes in Mathematical Modeling*. Bremen University, 2002.

[6] M. Böhm, J. Devinny, F. Jahani, G. Rosen, On a moving-boundary system modeling corrosion in sewer pipes. *Appl. Math. Comput.* **92**:247-269 (1998).

[7] M. Böhm, I. G. Rosen, Global weak solutions and uniqueness for a moving boundary problem for a coupled system of quasilinear diffusion-reaction equations arising as a model of chemical corrosion of concrete surfaces. Part 3, preprint, Humbold University, Berlin, 1997.

[8] M. Böhm, J. Kropp, A. Muntean, A two-reaction-zones interface model for predicting $Ca(OH)_2$ carbonation in concrete. in preparation.

[9] M. Böhm, A. Muntean, Well-posedness of a reaction-layer model for predicting $Ca(OH)_2$ carbonation in concrete and a limit case. in preparation.

[10] M. Boulfiza, K. Sakai, N. Banthia, H. Yoshida, Synergetic effects of carbonation and chloride ions attacks in concrete structures. in press.

[11] L. M. Brieger, F. H. Wittmann, Numerical simulation of concrete carbonation, in *Werkstoffwissenschaften und Bausanierung, Berichtstand zum 2. Int. Koll.* (F. H. Wittmann, Ed.), Technische Akademie Esslingen, 1986.

[12] J. H. Cahyadi, T. Uomoto, Influence of Environmental Relative Humidity on Carbonation of Concrete (Mathematical Modeling), in *Durability of Building Materials and Components*, No. 6, Omiya, Japan, 1993.

[13] T. Chaussadent, États des lieux et réflexions sur la carbonatation du béton armé. LCPC OA29, Laboratoire Central des Ponts et Chaussées, Paris, 1999.

[14] J. Crank, *Free and Moving Boundary Problems*. Clarendon Press, Oxford, 1984.

[15] J. Crank, *The Mathematics of Diffusion*. Oxford Science Publications, Clarendon Press, Oxford, 1973.

[16] *CRC Handbook of Chemistry and Physics*. (D. R. Lide, Ed.), CRC Press LLC, 2001-2002.

[17] R. M. E. Diamant, *The Chemistry of Building Materials*. Business Brooks Ltd., London, 1970.

[18] L. Franke, K. Sisomphon, A new chemical method for analyzing free calcium hydroxide content in cementing material. submitted for publication, (2002).

[19] R. Gatignol, R. Prud'homme, *Mechanical and Thermodynamical Modeling of Fluid Interfaces.* World Scientific, Vol. 58, Singapore-New Jersey-London-Hong Kong, 2001.

[20] C. Gehlen, Lebensdauerbemessung- Zuverlassigkeitsberechnungen zur wirksamen Vermeidung von verschiedenartig induzierter Bewehrungskorrosion. *Beton-und Stahlbetonbau.* **7**:478-486 (2001).

[21] M. E. Gurtin, *Thermomechanics of Evolving Phase Boundaries in the Plane.* Oxford Science Publishers, Clarendon Press, Oxford, 1993.

[22] J. Grunewald *Documentation of the numerical simulation program DIM 3.1. Theoretical Fundamentals.* vol. 1, 2000.

[23] J. Grunewald, Mass and energy transport in porous media – Thermodynamical identification of driving potentials. *Internationale Zeitschrift für Bauinstandsetzen und Baudenkmalpflege.* **2**:113-142 (1999).

[24] R. Hohmann, M. J. Setzer, *Bauphysikalische Formeln und Tabellen.* Werner Verlag, Düsseldorf, 1995.

[25] Y. F. Houst, P. E. Roelfstra, F. H. Wittmann, A model to predict service life of concrete structures, in Werkstoffwissenschaften und Bausanierung. Berichtstand zum 2. Int. Koll. (F. H. Wittmann, Ed.), Technische Akademie Esslingen, 1986.

[26] Y. F. Houst, P. E. Roelfstra, F. H. Wittmann, A model to predict service life of concrete structures, in *Proc. Conf. Techn. Akademie Esslingen*, 1983.

[27] Y. F. Houst, The role of moisture in the carbonation of cementitious materials. *Internationale Zeitschrift für Bauinstandsetzen.* **2**:49-66 (1996).

[28] Y. F. Houst, F. H. Wittmann, Depth profiles of carbonates formed during natural carbonation. *Cem. Concr. Res.* **32**:1923-1930 (2002).

[29] T. Ishida, K. Maekawa, Modeling of pH profile in pore water based on mass transport and chemical equilibrium theory. *Concrete Library of JSCE.* **37**: 131-146 (2001).

[30] B. Johannesson, Modeling of transport processes involved in service life prediction of concrete. Important principles. Licentiate Thesis, Lund Institute of Technology, 1999.

[31] H. Knoblauch, U. Schneider, *Bauchemie.* Werner Verlag, Düsseldorf, 1987.

[32] J. Kropp, *Relations between transport characteristics and durability,* in *Performance Criteria for Concrete Durability* (J. Kropp and H. K. Hilsdorf, Eds.), RILEM **12**:97-137 (1995).

[33] J. Kropp, Private communications, (2003).

[34] J. Kropp, Karbonatisierung und Transportvorgänge in Zementstein. Ph. D. Thesis, Karlsruhe, 1983.

[35] G. H. Landau, Heat conduction in a melting solid. *Quart. Appl. Mech. Math.* **8**:81-94 (1950).

[36] M. Mainguy, Modèles de diffusion non-linéaires en milieux poreux. Application à la dissolution et au séchage des matériaux cimentaires. Ph. D. Thesis, École Nationale des Ponts et Chaussées, 1999.

[37] M. Mainguy, O. Coussy, Propagation fronts during calcium leaching and chloride penetration, *J. Engng. Mech.* **126**:250-257 (2000).

[38] K. Maekawa, T. Ishida, Service-life evaluation of reinforced concrete under coupled forces and environmental actions, in *Transport in Cement-Based Materials, Materials Science of Concrete, Ion and Mass Transport*, The American Ceramic Society, 2000.

[39] J. Marchand, Modeling the behavior of unsaturated cement systems exposed to aggresive chemical environments. *Materials and Structures/Matériaux et Constructions.* **34**:195-200 (2001).

[40] A. M. Meirmanov, *The Stefan Problem.* De Gruyter Expositions in Mathematics, Berlin-New York, 1992.

[41] P. Moszkovicz, J. Pousin, F. Sanchez, Diffusion and dissolution in a reactive porous medium: Mathematical modeling and numerical simulations. *J. Comp. Appl. Math.* **66**:377-389 (1996).

[42] A. M. Neville, *Concrete Technology.* Pearson Higher Education, N.Y., 1994.

[43] J. Ockendon, S. Howison, A. Lacey, A. Movchan, *Applied Partial Differential Equations.* Oxford University Press, Oxford, 1999.

[44] P. Ortoleva, G. Auchmuty, J. Chadam, J. Hettmer, E. Merino, C. H. Moore, Redox front propagation and banding modalities. *Physica D.* **19**:334-354 (1986).

[45] V. G. Papadakis, C. G. Vayenas, M. N. Fardis, A reaction engineering approach to the problem of concrete carbonation. *AIChE Journal.* **35**:1639-1650 (1989).

[46] V. G. Papadakis, C. G. Vayenas, M. N. Fardis, Physical and chemical characteristics affecting the durability of concrete. *ACI Materials Journal.* **88**:186-196 (1991).

[47] V. G. Papadakis, C. G. Vayenas, M. N. Fardis, Fundamental modeling and experimental investigation of concrete carbonation. *ACI Materials Journal.* **88**:363-373 (1991).

[48] A. Pawell, K.-D. Krannich, Dissolution effects in transport in porous media. *SIAM J. Appl. Math.* **56**:89-118 (1996).

[49] P. M. Raviart, J. M. Thomas, *Introduction à l'Analyse Numérique des Équations aux Dérivées Partielles.* Editions Masson, Paris, 1983.

[50] J. Rubin, C. Wallis, Transport of reacting solutes subject to a moving dissolution boundary: Numerical methods and solutions. *Water Resources Research*, **23**:1231-1252 (1983).

[51] L. I. Rubinstein, *The Stefan Problem.* Transl. Math. Monographs, AMS, vol. 27, 1971.

[52] T. Saeki, H. Ohga, S. Nagataki, Mechanism of carbonation and prediction of carbonation process of concrete. *Concrete Library of JSCE.* **17**:23-36 (1991).

[53] A. V. Saetta, B. A. Schrefler, R. V. Vitaliani, The carbonation of concrete and the mechanism of moisture, heat and carbon dioxide flow through porous materials. *Cem. Concr. Res.* **23**:761-772 (1993).

[54] A. V. Saetta, B. A. Schrefler, R. V. Vitaliani, 2-D model for carbonation and moisture/heat flow in porous materials. *Cem. Concr. Res.* **25**:1703-1712 (1995).

[55] E. Samson, J. Marchand, J. J. Beaudoin, Describing ion diffusion in cement-based materials using the homogenization technique. *Cem Concr. Res.* **29**:1341-1345 (1999).

[56] M. J. Setzer, U. Dahme, In preparation, 2003.

[57] L. F. Shampine, M. W. Reichelt, The MATLAB ode suite. *SIAM J. Sci. Comput.* **18**:1-22 (1997).

[58] K. Sisomphon, L. Franke, Private communications. (2003).

[59] A. Steffens, D. Dinkler, H. Ahrens, Modeling carbonation for corrosion risk prediction of concrete structures. *Cem. Concr. Res.* **32**:935-941 (2002).

[60] A. Steffens, Modellierung von Karbonatisierung und Chloridbindung zur numerischen Analyse der Korrosionsgefährdung der Betonbewehrung. PhD. Thesis, Technical University of Braunschweig, 2000.

[61] H. F. W. Taylor, *Cement Chemistry.* Thomas Telford Publishing, London, 1997.

[62] R. Temam, A. Miranville, *Mathematical Modeling in Continuum Mechanics.* Cambridge University Press, Cambridge, 2001.

**Berichte aus der Technomathematik** ISSN 1435-7968

http://www.math.uni-bremen.de/zetem/berichte.html

— Vertrieb durch den Autor —

**Reports** **Stand: 16. April 2003**

98–01. Peter Benner, Heike Faßbender:
*An Implicitly Restarted Symplectic Lanczos Method for the Symplectic Eigenvalue Problem*, Juli 1998.

98–02. Heike Faßbender:
*Sliding Window Schemes for Discrete Least-Squares Approximation by Trigonometric Polynomials*, Juli 1998.

98–03. Peter Benner, Maribel Castillo, Enrique S. Quintana-Ortí:
*Parallel Partial Stabilizing Algorithms for Large Linear Control Systems*, Juli 1998.

98–04. Peter Benner:
*Computational Methods for Linear–Quadratic Optimization*, August 1998.

98–05. Peter Benner, Ralph Byers, Enrique S. Quintana-Ortí, Gregorio Quintana-Ortí:
*Solving Algebraic Riccati Equations on Parallel Computers Using Newton's Method with Exact Line Search*, August 1998.

98–06. Lars Grüne, Fabian Wirth:
*On the rate of convergence of infinite horizon discounted optimal value functions*, November 1998.

98–07. Peter Benner, Volker Mehrmann, Hongguo Xu:
*A Note on the Numerical Solution of Complex Hamiltonian and Skew-Hamiltonian Eigenvalue Problems*, November 1998.

98–08. Eberhard Bänsch, Burkhard Höhn:
*Numerical simulation of a silicon floating zone with a free capillary surface*, Dezember 1998.

99–01. Heike Faßbender:
*The Parameterized SR Algorithm for Symplectic (Butterfly) Matrices*, Februar 1999.

99–02. Heike Faßbender:
*Error Analysis of the symplectic Lanczos Method for the symplectic Eigenvalue Problem*, März 1999.

99–03. Eberhard Bänsch, Alfred Schmidt:
*Simulation of dendritic crystal growth with thermal convection*, März 1999.

99–04. Eberhard Bänsch:
*Finite element discretization of the Navier-Stokes equations with a free capillary surface*, März 1999.

99–05. Peter Benner:
*Mathematik in der Berufspraxis*, Juli 1999.

99–06. Andrew D.B. Paice, Fabian R. Wirth:
*Robustness of nonlinear systems and their domains of attraction*, August 1999.

99–07. Peter Benner, Enrique S. Quintana-Ortí, Gregorio Quintana-Ortí:
*Balanced Truncation Model Reduction of Large-Scale Dense Systems on Parallel Computers*, September 1999.

99–08. Ronald Stöver:
*Collocation methods for solving linear differential-algebraic boundary value problems*, September 1999.

99–09. Huseyin Akcay:
*Modelling with Orthonormal Basis Functions*, September 1999.

99–10. Heike Faßbender, D. Steven Mackey, Niloufer Mackey:
*Hamilton and Jacobi come full circle: Jacobi algorithms for structured Hamiltonian eigenproblems*, Oktober 1999.

99–11. Peter Benner, Vincente Hernández, Antonio Pastor:
*On the Kleinman Iteration for Nonstabilizable System*, Oktober 1999.

99–12. Peter Benner, Heike Faßbender:
*A Hybrid Method for the Numerical Solution of Discrete-Time Algebraic Riccati Equations*, November 1999.

99–13. Peter Benner, Enrique S. Quintana-Ortí, Gregorio Quintana-Ortí:
*Numerical Solution of Schur Stable Linear Matrix Equations on Multicomputers*, November 1999.

99–14. Eberhard Bänsch, Karol Mikula:
*Adaptivity in 3D Image Processing*, Dezember 1999.

00–01. Peter Benner, Volker Mehrmann, Hongguo Xu:
*Perturbation Analysis for the Eigenvalue Problem of a Formal Product of Matrices*, Januar 2000.

00–02. Ziping Huang:
*Finite Element Method for Mixed Problems with Penalty*, Januar 2000.

00–03. Gianfrancesco Martinico:
*Recursive mesh refinement in 3D*, Februar 2000.

00–04. Eberhard Bänsch, Christoph Egbers, Oliver Meincke, Nicoleta Scurtu:
*Taylor-Couette System with Asymmetric Boundary Conditions*, Februar 2000.

00–05. Peter Benner:
*Symplectic Balancing of Hamiltonian Matrices*, Februar 2000.

00–06. Fabio Camilli, Lars Grüne, Fabian Wirth:
*A regularization of Zubov's equation for robust domains of attraction*, März 2000.

00–07. Michael Wolff, Eberhard Bänsch, Michael Böhm, Dominic Davis:
*Modellierung der Abkühlung von Stahlbrammen*, März 2000.

00–08. Stephan Dahlke, Peter Maaß, Gerd Teschke:
*Interpolating Scaling Functions with Duals*, April 2000.

00–09. Jochen Behrens, Fabian Wirth:
*A globalization procedure for locally stabilizing controllers*, Mai 2000.

00–10. Peter Maaß, Gerd Teschke, Werner Willmann, Günter Wollmann:
*Detection and Classification of Material Attributes – A Practical Application of Wavelet Analysis*, Mai 2000.

00–11. Stefan Boschert, Alfred Schmidt, Kunibert G. Siebert, Eberhard Bänsch, Klaus-Werner Benz, Gerhard Dziuk, Thomas Kaiser:
*Simulation of Industrial Crystal Growth by the Vertical Bridgman Method*, Mai 2000.

00–12. Volker Lehmann, Gerd Teschke:
*Wavelet Based Methods for Improved Wind Profiler Signal Processing*, Mai 2000.

00–13. Stephan Dahlke, Peter Maass:
*A Note on Interpolating Scaling Functions*, August 2000.

00–14. Ronny Ramlau, Rolf Clackdoyle, Frédéric Noo, Girish Bal:
*Accurate Attenuation Correction in SPECT Imaging using Optimization of Bilinear Functions and Assuming an Unknown Spatially-Varying Attenuation Distribution*, September 2000.

00–15. Peter Kunkel, Ronald Stöver:
*Symmetric collocation methods for linear differential-algebraic boundary value problems*, September 2000.

00–16. Fabian Wirth:
*The generalized spectral radius and extremal norms*, Oktober 2000.

00–17. Frank Stenger, Ahmad Reza Naghsh-Nilchi, Jenny Niebsch, Ronny Ramlau:
*A unified approach to the approximate solution of PDE*, November 2000.

00–18. Peter Benner, Enrique S. Quintana-Ortí, Gregorio Quintana-Ortí:
*Parallel algorithms for model reduction of discrete–time systems*, Dezember 2000.

00–19. Ronny Ramlau:
*A steepest descent algorithm for the global minimization of Tikhonov–Phillips functional*, Dezember 2000.

01–01. Efficient methods in hyperthermia treatment planning:
*Torsten Köhler, Peter Maass, Peter Wust, Martin Seebass*, Januar 2001.

01–02. Parallel Algorithms for LQ Optimal Control of Discrete-Time Periodic Linear Systems:
*Peter Benner, Ralph Byers, Rafael Mayo, Enrique S. Quintana-Ortí, Vicente Hernández*, Februar 2001.

01–03. Peter Benner, Enrique S. Quintana-Ortí, Gregorio Quintana-Ortí:
*Efficient Numerical Algorithms for Balanced Stochastic Truncation*, März 2001.

01–04. Peter Benner, Maribel Castillo, Enrique S. Quintana-Ortí:
*Partial Stabilization of Large-Scale Discrete-Time Linear Control Systems*, März 2001.

01–05. Stephan Dahlke:
*Besov Regularity for Edge Singularities in Polyhedral Domains*, Mai 2001.

01–06. Fabian Wirth:
*A linearization principle for robustness with respect to time-varying perturbations*, Mai 2001.

01–07. Stephan Dahlke, Wolfgang Dahmen, Karsten Urban:
*Adaptive Wavelet Methods for Saddle Point Problems - Optimal Convergence Rates*, Juli 2001.

01–08. Ronny Ramlau:
*Morozov's Discrepancy Principle for Tikhonov regularization of nonlinear operators*, Juli 2001.

01–09. Michael Wolff:
*Einführung des Drucks für die instationären Stokes–Gleichungen mittels der Methode von Kaplan*, Juli 2001.

01–10. Stephan Dahlke, Peter Maaß, Gerd Teschke:
*Reconstruction of Reflectivity Desities by Wavelet Transforms*, August 2001.

01–11. Stephan Dahlke:
*Besov Regularity for the Neumann Problem*, August 2001.

01–12. Bernard Haasdonk, Mario Ohlberger, Martin Rumpf, Alfred Schmidt, Kunibert G. Siebert:
*h–p–Multiresolution Visualization of Adaptive Finite Element Simulations*, Oktober 2001.

01–13. Stephan Dahlke, Gabriele Steidl, Gerd Teschke:
*Coorbit Spaces and Banach Frames on Homogeneous Spaces with Applications to Analyzing Functions on Spheres*, August 2001.

02–01. Michael Wolff, Michael Böhm:
*Zur Modellierung der Thermoelasto-Plastizität mit Phasenumwandlungen bei Stählen sowie der Umwandlungsplastizität*, Februar 2002.

02–02. Stephan Dahlke, Peter Maaß:
*An Outline of Adaptive Wavelet Galerkin Methods for Tikhonov Regularization of Inverse Parabolic Problems*, April 2002.

02–03. Alfred Schmidt:
*A Multi-Mesh Finite Element Method for Phase Field Simulations*, April 2002.

02–04. Sergey N. Dachkovski, Michael Böhm:
*A Note on Finite Thermoplasticity with Phase Changes*, Juli 2002.

02–05. Michael Wolff, Michael Böhm:
*Phasenumwandlungen und Umwandlungsplastizität bei Stählen im Konzept der Thermoelasto-Plastizität*, Juli 2002.

02–06. Gerd Teschke:
*Construction of Generalized Uncertainty Principles and Wavelets in Anisotropic Sobolev Spaces*, August 2002.

02–07. Ronny Ramlau:
*TIGRA – an iterative algorithm for regularizing nonlinear ill–posed problems*, August 2002.

02–08. Michael Lukaschewitsch, Peter Maaß, Michael Pidcock:
*Tikhonov regularization for Electrical Impedance Tomography on unbounded domains*, Oktober 2002.

02–09. Volker Dicken, Peter Maaß, Ingo Menz, Jenny Niebsch, Ronny Ramlau:
*Inverse Unwuchtidentifikation an Flugtriebwerken mit Quetschöldämpfern*, Oktober 2002.

02–10. Torsten Köhler, Peter Maaß, Jan Kalden:
*Time-series forecasting for total volume data and charge back data*, November 2002.

02–11. Angelika Bunse-Gerstner:
*A Short Introduction to Iterative Methods for Large Linear Systems*, November 2002.

02–12. Peter Kunkel, Volker Mehrmann, Ronald Stöver:
*Symmetric Collocation for Unstructured Nonlinear Differential-Algebraic Equations of Arbitrary Index*, November 2002.

02–13. Michael Wolff:
*Ringvorlesung: Distortion Engineering 2*
*Kontinuumsmechanische Modellierung des Materialverhaltens von Stahl unter Berücksichtigung von Phasenumwandlungen*, Dezember 2002.

02–14. Michael Böhm, Martin Hunkel, Alfred Schmidt, Michael Wolff:
*Evaluation of various phase-transition models for 100Cr6 for application in commercial FEM programs*, Dezember 2002.

03–01. Michael Wolff, Michael Böhm, Serguei Dachkovski:
*Volumenanteile versus Massenanteile - der Dilatometerversuch aus der Sicht der Kontinuumsmechanik*, Januar 2003.

03–02. Daniel Kessler, Ricardo H. Nochetto, Alfred Schmidt:
*A posteriori error control for the Allen-Cahn Problem: circumventing Gronwall's inequality*, März 2003.

03–03. Michael Böhm, Jörg Kropp, Adrian Muntean:
*On a Prediction Model for Concrete Carbonation based on Moving Interfaces - Interface concentrated Reactions*, April 2003.

03–04. Michael Böhm, Jörg Kropp, Adrian Muntean:
*A Two-Reaction-Zones Moving-Interface Model for Predicting $Ca(OH)_2$ Carbonation in Concrete*, April 2003.